

Intelligent Reflecting Surface Aided Full-Duplex Communication: Passive Beamforming and Deployment Design

Yunlong Cai, *Senior Member, IEEE*, Ming-Min Zhao, *Member, IEEE*, Kaidi Xu, and Rui Zhang, *Fellow, IEEE*

Abstract

This paper investigates the passive beamforming and deployment design for an intelligent reflecting surface (IRS) aided full-duplex (FD) wireless system, where an FD access point (AP) communicates with an uplink (UL) user and a downlink (DL) user simultaneously over the same time-frequency dimension with the help of IRS. Under this setup, we consider three deployment cases: 1) two distributed IRSs placed near the UL user and DL user, respectively; 2) one centralized IRS placed near the DL user; 3) one centralized IRS placed near the UL user. In each case, we aim to minimize the weighted sum transmit power consumption of the AP and UL user by jointly optimizing their transmit power and the passive reflection coefficients at the IRS (or IRSs), subject to the UL and DL users' rate constraints and the uni-modulus constraints on the IRS reflection coefficients. First, we analyze the minimum transmit power required in the IRS-aided FD system under each deployment scheme, and compare it with that of the corresponding half-duplex (HD) system. We show that the FD system outperforms its HD counterpart for all IRS deployment schemes, while the distributed deployment further outperforms the other two centralized deployment schemes. Next, we transform the challenging power minimization problem into an equivalent but more tractable form and propose an efficient algorithm to solve it based on the block coordinate descent (BCD) method. Finally, numerical results are presented to validate our analysis as well as the efficacy of the proposed passive beamforming design.

Index Terms

Intelligent reflecting surface, full-duplex, passive beamforming, deployment, power minimization.

Y. Cai, M. Zhao, and K. Xu are with the College of Information Science and Electronic Engineering, Zhejiang University, China (e-mail: ylcai@zju.edu.cn; zmmblack@zju.edu.cn; xukaidi13@126.com). R. Zhang is with the Department of Electrical and Computer Engineering, National University of Singapore, Singapore (e-mail: elezhang@nus.edu.sg).

I. INTRODUCTION

Recently, intelligent reflecting surface (IRS) and its various equivalents have emerged as a promising technology to enhance the spectral efficiency of wireless communication systems with low hardware cost and energy consumption [1]–[5]. Specifically, IRS is generally equipped with a planar surface composed of a large number of passive reflecting elements, each of which can induce an independent phase shift and/or amplitude change of the incident signal in real time. Based on the channel state information (CSI) and with the aid of a smart controller, IRS is able to modify/reconfigure the signal propagation by dynamically adjusting its reflection coefficients such that the desired and interfering signals can be added constructively and destructively at the receivers, respectively, to boost the desired signal power and/or suppress the co-channel interference (CCI), thus achieving communication performance improvement. Additionally, since such passive reflecting elements do not require any active transmit radio frequency (RF) chains (which constitute high-cost amplifiers, filters, mixers, attenuators and detectors, etc.), their energy and hardware costs are much lower than those of the active components in traditional base stations (BSs), access points (APs), and relays. As a result, IRSs can be flexibly deployed in wireless networks and seamlessly integrated into the existing cellular or WiFi systems, with controllable interference to each other as they usually have much smaller signal coverage than active BSs/APs/relays. Due to the above advantages, IRS has been extensively studied under various setups (see, e.g., [6]–[11]), where the effectiveness of IRS in enhancing these systems' performance was demonstrated.

To boost the spectral efficiency of wireless systems, the full-duplex (FD) communication is another promising technique [12]–[14]. Compared with the traditional half-duplex (HD) system, it better utilizes the spectrum by enabling signal transmission and reception over the same time-frequency dimension and thus can double the spectral efficiency theoretically. Although the FD system offers promising spectral efficiency gains, it also brings challenges in practice, such as the self-interference (SI) and CCI caused by the simultaneous downlink (DL) and uplink (UL) transmissions. These interferences, if left unattended, can encroach the gain offered by FD and even degrade the system performance as compared to traditional HD. Fortunately, many efficient SI cancellation techniques have been proposed in the literature [14]–[16], such as passive suppression, analog and digital cancellations, etc., and it has been reported that the SI can be suppressed up to the background noise floor at an FD node [17], which leads to implementable FD systems. However, the CCI inherited from the FD operation can also cause significant spectral

efficiency degradation, despite the fact that the SI can be effectively suppressed. In practice, the interference from the UL users to the DL users (UL-to-DL interference) can be detrimental if the UL and DL users are located close to each other. To avoid the performance degradation due to CCI, various methods such as DL/UL user pairing and transmission scheduling have been proposed in the literature (see e.g., [18], [19] and the references therein).

Motivated by the above, in this paper, we combine the two spectral-efficient wireless techniques, i.e., IRS and FD into a new system, which can leverage IRS's interference cancellation and signal enhancement capabilities to further improve the FD communication performance.

A. Prior Works

IRS has been studied recently in various wireless systems, such as IRS-aided orthogonal frequency division multiplexing (OFDM) [10], mmWave communication [20], [21], physical layer security [22], [23], wireless power transfer [24], [25], etc. To the best of our knowledge, there are only few works that have studied IRS-aided FD systems [26]–[28]. Specifically, in [26], the authors studied an IRS-aided FD multiple-input multiple-output (MIMO) two-way communication system and the sum-rate maximization problem was considered by jointly optimizing the active precoders at the sources and the IRS reflection coefficients through the Arimoto-Blahut algorithm. Under the same system model, the authors in [27] further proposed an alternating optimization algorithm to solve the sum-rate maximization problem with lower computational complexity. In [28], an IRS-assisted FD cognitive radio system was investigated, where the IRS is employed to enhance the performance of the secondary network and in the meantime mitigate the interference caused to the primary users. Note that these existing works on IRS-aided FD systems mainly focused on joint active and passive beamforming design, while the fundamental advantages of IRS-aided FD versus HD system are not fully characterized yet. Moreover, with a given number of IRS reflecting elements, there are various IRS deployment strategies for an IRS-aided FD system, e.g., placing multiple IRSs in the network for far-apart users separately, or forming them as one large IRS and placing it near a cluster of nearby users, which are referred to as distributed and centralized deployment, respectively. The IRS deployment problem has been investigated in the point-to-point channel [29] and the UL (DL) multiple access (broadcast) channel [30]; while it is yet unclear which of the above two IRS deployment strategies (centralized or distributed) achieves better performance in IRS-aided FD systems.

B. Main Contributions

In this paper, we consider an IRS-aided FD system where an FD AP (equipped with one transmit antenna and one receive antenna) communicates with a single-antenna UL user and a single-antenna DL user simultaneously over the same time-frequency dimension with the help of a given number of IRS reflecting elements. For simplicity, we assume that the IRS (or IRSs if deployed in a distributed manner) is placed in close vicinity to the users to minimize the path loss. Under this setup, we investigate three deployment cases: 1) two distributed IRSs placed near the UL user and DL user, respectively; 2) one centralized IRS placed near the DL user; and 3) one centralized IRS placed near the UL user. In each case, we aim to minimize the weighted sum transmit power consumption of the AP and UL user by jointly optimizing their transmit power and the passive reflection coefficients at the IRS (or IRSs), subject to the UL and DL users' rate constraints and the uni-modulus constraints on the IRS reflection coefficients. To focus on the deployment strategy design and passive beamforming optimization, we assume for simplicity the availability of CSI for all channels involved, which can be obtained by various existing channel estimation methods (e.g., [10], [31], [32]). The main contributions of this paper in view of the existing literature are summarized as follows.

- First, by assuming Rayleigh fading channels and with an asymptotically large number of IRS reflecting elements, we analyze the minimum transmit power required in the above-mentioned three IRS deployment cases. In particular, we show that with the aid of IRS, the FD system always outperforms the HD system regardless of the UL-to-DL interference. This is in sharp contrast with the conventional system without IRS, where the FD operation is not always beneficial, especially in the case that the UL-to-DL interference is severe. Besides, we show that the minimum power consumption with the distributed deployment (Case 1) is much lower than that with the centralized deployment (Case 2 or 3) in the IRS-aided FD system, which unveils that the distributed deployment generally outperforms centralized deployment in terms of power consumption.
- Second, for arbitrary channels and finite number of reflecting elements, we propose an efficient passive beamforming design algorithm for solving the formulated power minimization problem, which is difficult to solve due to the non-convex objective function and uni-modulus constraints. Specifically, we first transform the original problem into an equivalent but more tractable form by introducing an auxiliary variable, and then propose an algorithm for solving it by employing the block coordinate descent (BCD) method. The computational

complexity and convergence property of the proposed algorithm are analyzed.

- Finally, numerical results are presented to validate our analysis and show the performance of the proposed algorithm. Particularly, we draw useful insights into the impact of the distance between the UL and DL users, the number of reflecting elements and the UL/DL target rates on the total transmit power. Besides, performance comparison between the proposed algorithm and a low-complexity heuristic algorithm is provided.

C. Organization

The rest of this paper is organized as follows. Section II describes the system model and formulates the optimization problem of interest. In Section III, we analyze the minimum power consumption for FD and HD systems under different IRS deployment cases. In Section IV, we propose a new algorithm to optimize the passive beamforming for solving the formulated problems. The simulation results are presented in Section V and our conclusions are drawn in Section VI.

Notations: Scalars, vectors and matrices are respectively denoted by lower case, boldface lower case and boldface upper case letters. \mathbf{I} represents an identity matrix and $\mathbf{0}$ denotes an all-zero matrix. For a matrix \mathbf{A} , \mathbf{A}^T , $\text{conj}(\mathbf{A})$, \mathbf{A}^H and $\|\mathbf{A}\|$ denote its transpose, conjugate, conjugate transpose and Frobenius norm, respectively. $\text{diag}(\mathbf{A})$ denotes a vector whose elements are the corresponding ones on the main diagonal of \mathbf{A} . For a vector \mathbf{a} , $\text{Diag}(\mathbf{a})$ denotes a diagonal matrix with each diagonal element being the corresponding element in \mathbf{a} . $\mathbf{1}$ denotes an all-ones vector. $\Re\{\cdot\}$ ($\Im\{\cdot\}$) denotes the real (imaginary) part of a variable, while $|\cdot|$ represents the absolute value of a complex scalar. $\mathbb{C}^{m \times n}$ ($\mathbb{R}^{m \times n}$) denotes the space of $m \times n$ complex (real) matrices. The letter j is used to represent $\sqrt{-1}$ when there is no ambiguity. \mathbb{Z}^+ denotes a set of positive integers. The operator \angle takes the phase angles of the elements in a matrix. $\mathbf{a} \sim \mathcal{CN}(\mathbf{0}, \mathbf{A})$ denotes that the random vector \mathbf{a} follows the circularly-symmetric complex Gaussian distribution with zero mean and covariance matrix \mathbf{A} .

II. SYSTEM MODEL AND PROBLEM FORMULATION

In this section, we introduce the system model and problem formulation for three different IRS deployment cases under investigation.

A. FD System

Consider an FD system consisting of an AP, a UL user and a DL user. The AP is equipped with a single transmit antenna and a receive antenna, and operates in the FD mode. The UL and DL users are both equipped with a single antenna, and operate in the HD mode.¹

Generally, IRS is deployed near the users for enhancing their performance. Assuming a total of $N \in \mathbb{Z}^+$ IRS reflecting elements utilized in the system, for this case depicted in Fig. 1 (a), there are two IRSs, namely IRS 1 and IRS 2, which are equipped with $\rho N \in \mathbb{Z}^+$ and $(1 - \rho)N \in \mathbb{Z}^+$ reflecting elements and deployed near the UL/DL user, respectively, where $0 < \rho < 1$ denotes a preset ratio. Since IRS 1 and IRS 2 are sufficiently far from the DL user and the UL user, respectively, the link that IRS 1 reflects the signals from the AP to the DL user as well as that IRS 2 reflects the signals from the UL user to the AP can be neglected, as compared to the other links shown in the figure. The received signal at the AP is expressed as

$$y_A = h_{AU}\sqrt{p_U}s_U + \mathbf{f}_{AI}^H \Theta_U \mathbf{f}_{IU}\sqrt{p_U}s_U + n_A, \quad (1)$$

where s_U denotes the transmit signal of the UL user, $p_U > 0$ denotes the transmit power of the UL user, and $n_A \in \mathbb{C}$ denotes the independent and identically distributed (i.i.d.) complex Gaussian noise at the AP with zero mean and variance σ_A^2 . $\mathbf{f}_{IU} \in \mathbb{C}^{\rho N \times 1}$ and $\mathbf{f}_{AI} \in \mathbb{C}^{\rho N \times 1}$ denote respectively the channel vector between the UL user and IRS 1, and that between IRS 1 and the AP. $h_{AU} \in \mathbb{C}$ denotes the channel coefficient between the UL user and the AP. $\Theta_U \in \mathbb{C}^{\rho N \times \rho N}$ denotes the passive beamforming matrix at IRS 1 placed near the UL user, which is a diagonal matrix due to no signal coupling/joint processing over its passive reflecting elements. Since the CSI of the SI link can be obtained at the AP, based on certain interference cancellation techniques [33], [34], we assume that the SI at the AP can be eliminated completely for the sake of exposition.

On the other hand, the received signal at the DL user is given by

$$y_D = h_{DA}\sqrt{p_A}s_D + \mathbf{g}_{DI}^H \Theta_D \mathbf{g}_{IA}\sqrt{p_A}s_D + \underbrace{g\sqrt{p_U}s_U + \mathbf{f}_{DI}^H \Theta_U \mathbf{f}_{IU}\sqrt{p_U}s_U + \mathbf{g}_{DI}^H \Theta_D \mathbf{g}_{IU}\sqrt{p_U}s_U}_{\text{interference from the UL user}} + n_D, \quad (2)$$

where s_D and $p_A > 0$ denote the transmit signal for the DL user and the transmit power at the AP, respectively. $\mathbf{g}_{IA} \in \mathbb{C}^{(1-\rho)N \times 1}$, $\mathbf{g}_{DI} \in \mathbb{C}^{(1-\rho)N \times 1}$, $\mathbf{f}_{DI} \in \mathbb{C}^{\rho N \times 1}$ and $\mathbf{g}_{IU} \in \mathbb{C}^{(1-\rho)N \times 1}$

¹In order to focus on our study, we consider a typical single-antenna two-user FD system; while the results in this paper can be extended to the general setup of IRS-aided multi-antenna and/or multi-user FD systems, which are left for future work.

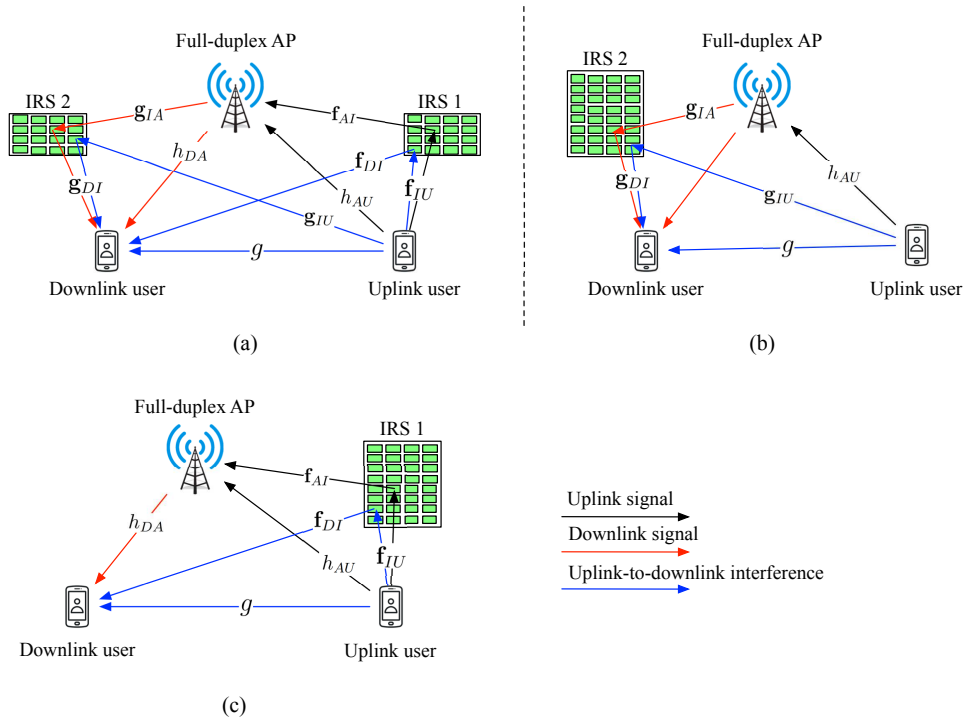


Fig. 1: (a) Case 1: IRSs placed near both users; (b) Case 2: IRS placed near the downlink user only; (c) Case 3: IRS placed near the uplink user only.

denote the channel vectors between the AP and IRS 2, between IRS 2 and the DL user, between IRS 1 and the DL user, and between the UL user and IRS 2, respectively. $h_{DA} \in \mathbb{C}$ denotes the channel coefficient between the AP and the DL user. $\Theta_D \in \mathbb{C}^{(1-\rho)N \times (1-\rho)N}$ denotes the diagonal beamforming matrix at IRS 2 which is placed near the DL user. g denotes the channel coefficient between the UL user and the DL user. $n_D \in \mathbb{C}$ denotes the i.i.d. complex Gaussian noise at the DL user with zero mean and variance σ_D^2 . The link between the two IRSs is also neglected due to their large distance and thus the high path loss.

Let us define the effective channel power gains, namely, $\lambda_D(\theta_D) \triangleq |h_{DA} + \mathbf{g}_{DA}^H \theta_D|^2$, where $\mathbf{g}_{DA} \triangleq \text{Diag}(\text{conj}(\mathbf{g}_{IA})) \mathbf{g}_{DI}$ and $\theta_D \triangleq \text{diag}(\Theta_D)$, $\lambda_U(\theta_U) \triangleq |h_{AU} + \mathbf{f}_{AU}^H \theta_U|^2$, where $\mathbf{f}_{AU} \triangleq \text{Diag}(\text{conj}(\mathbf{f}_{IU})) \mathbf{f}_{AI}$ and $\theta_U \triangleq \text{diag}(\Theta_U)$, and $\lambda_{DU}(\theta_U, \theta_D) \triangleq |g + \mathbf{d}^H \theta_{DU}|^2$, where $\theta_{DU} \triangleq [\theta_U^H, \theta_D^H]^H$, $\mathbf{d} \triangleq [\mathbf{f}_{DU}^H, \mathbf{g}_{DU}^H]^H$, $\mathbf{f}_{DU} \triangleq \text{Diag}(\text{conj}(\mathbf{f}_{IU})) \mathbf{f}_{DI}$, and $\mathbf{g}_{DU} \triangleq \text{Diag}(\text{conj}(\mathbf{g}_{IU})) \mathbf{g}_{DI}$. We aim to minimize the weighted sum transmit power consumption of the UL user and AP by jointly optimizing their corresponding transmit power levels p_U and p_A , and the passive beamforming vectors θ_U and θ_D at the two IRSs, subject to the UL and DL users' rate constraints and the uni-modulus constraints on the elements of the IRS passive beamforming vector. Accordingly,

the optimization problem is formulated as

$$\min_{p_U, p_A, \boldsymbol{\theta}_U, \boldsymbol{\theta}_D} \kappa_U p_U + \kappa_A p_A \quad (3a)$$

$$\text{s.t.} \quad \log \left(1 + \frac{p_U \lambda_U(\boldsymbol{\theta}_U)}{\sigma_A^2} \right) \geq \gamma_A, \quad (3b)$$

$$\log \left(1 + \frac{p_A \lambda_D(\boldsymbol{\theta}_D)}{p_U \lambda_{DU}(\boldsymbol{\theta}_U, \boldsymbol{\theta}_D) + \sigma_D^2} \right) \geq \gamma_D, \quad (3c)$$

$$|\boldsymbol{\theta}_U(n_1)| = 1, |\boldsymbol{\theta}_D(n_2)| = 1, \forall n_1 \in \{1, \dots, \rho N\}, \forall n_2 \in \{1, \dots, (1 - \rho)N\}, \quad (3d)$$

where we have assumed base-2 for the logarithm function, $\kappa_U > 0$ and $\kappa_A > 0$ represent the power weights corresponding to the UL user and AP, respectively. Constraints (3b) and (3c) correspond to the rate requirements for the UL and DL transmissions, respectively, where γ_A and γ_D denote the target rates in bits per second per Hertz (bits/s/Hz). (3d) denotes the uni-modulus constraints on all elements of the IRS passive beamforming vector.

Next, we consider two special cases of the general IRS deployment introduced in the above. First, for the case of placing all reflecting elements to IRS 2 near the DL user (i.e., with $\rho = 0$) as shown in Fig. 1 (b), let $\boldsymbol{\theta}_{DU} \in \mathbb{C}^{N \times 1}$ denote the entire passive beamforming vector at IRS 2. By defining $\tilde{\mathbf{g}}_{IA} \in \mathbb{C}^{N \times 1}$, $\tilde{\mathbf{g}}_{DI} \in \mathbb{C}^{N \times 1}$ and $\tilde{\mathbf{g}}_{IU} \in \mathbb{C}^{N \times 1}$ as the channel vectors between the AP and IRS 2, between IRS 2 and the DL user, and between the UL user and IRS 2, respectively, the optimization problem in this case can be formulated by simplifying (3) as

$$\min_{p_U, p_A, \boldsymbol{\theta}_{DU}} \kappa_U p_U + \kappa_A p_A \quad (4a)$$

$$\text{s.t.} \quad \log \left(1 + \frac{p_U |h_{AU}|^2}{\sigma_A^2} \right) \geq \gamma_A, \quad (4b)$$

$$\log \left(1 + \frac{p_A \omega_D(\boldsymbol{\theta}_{DU})}{p_U \omega_{DU}(\boldsymbol{\theta}_{DU}) + \sigma_D^2} \right) \geq \gamma_D, \quad (4c)$$

$$|\boldsymbol{\theta}_{DU}(n)| = 1, \forall n \in \{1, \dots, N\}. \quad (4d)$$

Here we have $\omega_D(\boldsymbol{\theta}_{DU}) \triangleq |h_{DA} + \tilde{\mathbf{g}}_{DA}^H \boldsymbol{\theta}_{DU}|^2$, where $\tilde{\mathbf{g}}_{DA} \triangleq \text{Diag}(\text{conj}(\tilde{\mathbf{g}}_{IA})) \tilde{\mathbf{g}}_{DI}$, and $\omega_{DU}(\boldsymbol{\theta}_{DU}) \triangleq |g + \tilde{\mathbf{g}}_{DU}^H \boldsymbol{\theta}_{DU}|^2$, where $\tilde{\mathbf{g}}_{DU} \triangleq \text{Diag}(\text{conj}(\tilde{\mathbf{g}}_{IU})) \tilde{\mathbf{g}}_{DI}$.

Second, for the other case of placing all reflecting elements to IRS 1 near the UL user (i.e., with $\rho = 1$) as depicted in Fig. 1 (c), let us define $\tilde{\mathbf{f}}_{IU} \in \mathbb{C}^{N \times 1}$ and $\tilde{\mathbf{f}}_{AI} \in \mathbb{C}^{N \times 1}$ as the channel vectors between the UL user and IRS 1 and between IRS 1 and the AP, respectively, and $\tilde{\mathbf{f}}_{DI} \in \mathbb{C}^{N \times 1}$

as the channel vector between IRS 1 and the DL user. Similarly, the optimization problem in this case can be formulated as

$$\min_{p_U, p_A, \boldsymbol{\theta}_{DU}} \kappa_U p_U + \kappa_A p_A \quad (5a)$$

$$\text{s.t.} \quad \log \left(1 + \frac{p_U \xi_U(\boldsymbol{\theta}_{DU})}{\sigma_A^2} \right) \geq \gamma_A, \quad (5b)$$

$$\log \left(1 + \frac{p_A |h_{DA}|^2}{p_U \xi_{DU}(\boldsymbol{\theta}_{DU}) + \sigma_D^2} \right) \geq \gamma_D, \quad (5c)$$

$$|\boldsymbol{\theta}_{DU}(n)| = 1, \forall n \in \{1, \dots, N\}. \quad (5d)$$

Here we define $\xi_U(\boldsymbol{\theta}_{DU}) \triangleq |h_{AU} + \tilde{\mathbf{f}}_{AU}^H \boldsymbol{\theta}_{DU}|^2$, where $\tilde{\mathbf{f}}_{AU} \triangleq \text{Diag}(\text{conj}(\tilde{\mathbf{f}}_{IU})) \tilde{\mathbf{f}}_{AI}$, and $\xi_{DU}(\boldsymbol{\theta}_{DU}) \triangleq |g + \tilde{\mathbf{f}}_{DU}^H \boldsymbol{\theta}_{DU}|^2$, where $\tilde{\mathbf{f}}_{DU} \triangleq \text{Diag}(\text{conj}(\tilde{\mathbf{f}}_{DI})) \tilde{\mathbf{f}}_{IU}$.

B. HD System

As for the corresponding HD system, the received signal vectors at the AP and DL user for the three deployment schemes are similar to that of the FD system, but there is no interference term from the UL user due to the orthogonal UL and DL transmissions. The detailed expressions of the received signals are thus omitted for brevity. As a result, the optimization problem of Case 1 in the HD system is expressed as

$$\min_{p_U, p_A, \boldsymbol{\theta}_U, \boldsymbol{\theta}_D} \kappa_U p_U + \kappa_A p_A \quad (6a)$$

$$\text{s.t.} \quad \frac{1}{2} \log \left(1 + \frac{p_U \lambda_U(\boldsymbol{\theta}_U)}{\frac{1}{2} \sigma_A^2} \right) \geq \gamma_A, \quad (6b)$$

$$\frac{1}{2} \log \left(1 + \frac{p_A \lambda_D(\boldsymbol{\theta}_D)}{\frac{1}{2} \sigma_D^2} \right) \geq \gamma_D, \quad (6c)$$

$$(3d),$$

where (6b) and (6c) denote the user rate constraints, and the factor $\frac{1}{2}$ is due to the fact that the uplink and downlink transmissions are allocated with either half of the bandwidth or half of the time as compared to the FD system. The optimization problems for Cases 2 and 3 in the HD system can be similarly formulated, thus they are omitted here.

In the following two sections, we first analyze the minimum power consumption required in different IRS deployment cases with given IRS passive beamforming vectors. Then, we propose an efficient algorithm to optimize the passive beamforming and thereby solve the above problems.

III. PERFORMANCE ANALYSIS

In this section, we analyze the minimum transmit power required in the IRS-aided FD system under each IRS deployment scheme, and compare it with that of the corresponding HD system. We show that the FD system outperforms its HD counterpart for all IRS deployment schemes, while the distributed deployment further outperforms the other two centralized deployment schemes in the IRS-aided FD system.

A. Comparison of FD versus HD Systems

In this subsection, we compare the power consumption of IRS-aided FD system with its HD counterpart under the three considered IRS deployment cases.

1) *Case 1*: First, consider the case of placing IRSs near both users as shown in Fig. 1 (a). For the FD system, since the user rates are monotonically increasing with p_U and p_A , their optimal solutions in (3) should guarantee that the inequality constraints (3b) and (3c) are met with equality. Thus, the optimal transmit power p_U^* and p_A^* are given by

$$p_U^* = \frac{(2^{\gamma_A} - 1)\sigma_A^2}{\lambda_U(\boldsymbol{\theta}_U)}, \quad (7)$$

$$p_A^* = \frac{(2^{\gamma_D} - 1)\sigma_A^2(2^{\gamma_A} - 1)\lambda_{DU}(\boldsymbol{\theta}_U, \boldsymbol{\theta}_D)}{\lambda_D(\boldsymbol{\theta}_D)\lambda_U(\boldsymbol{\theta}_U)} + \frac{(2^{\gamma_D} - 1)\sigma_D^2}{\lambda_D(\boldsymbol{\theta}_D)}. \quad (8)$$

By defining $\boldsymbol{\theta}_U^*$ and $\boldsymbol{\theta}_D^*$ as the optimal IRS passive beamforming/phase-shift vectors for Case 1, the minimum power consumption of the FD system can be expressed as

$$L_1(\boldsymbol{\theta}_U^*, \boldsymbol{\theta}_D^*) \triangleq \kappa_U p_U^* + \kappa_A p_A^* = \frac{\bar{\gamma}_1 \lambda_{DU}(\boldsymbol{\theta}_U^*, \boldsymbol{\theta}_D^*)}{\lambda_D(\boldsymbol{\theta}_D^*) \lambda_U(\boldsymbol{\theta}_U^*)} + \frac{\bar{\gamma}_2}{\lambda_D(\boldsymbol{\theta}_D^*)} + \frac{\bar{\gamma}_3}{\lambda_U(\boldsymbol{\theta}_U^*)}, \quad (9)$$

where $\bar{\gamma}_1 \triangleq \kappa_A(2^{\gamma_D} - 1)\sigma_A^2(2^{\gamma_A} - 1)$, $\bar{\gamma}_2 \triangleq \kappa_A(2^{\gamma_D} - 1)\sigma_D^2$ and $\bar{\gamma}_3 \triangleq \kappa_U(2^{\gamma_A} - 1)\sigma_A^2$.

By recalling problem (6), similarly, the minimum power consumption of the HD system in Case 1 can be expressed as

$$\tilde{L}_1(\boldsymbol{\theta}_U^{**}, \boldsymbol{\theta}_D^{**}) = \frac{\kappa_U(2^{2\gamma_A} - 1)\sigma_A^2}{2\lambda_U(\boldsymbol{\theta}_U^{**})} + \frac{\kappa_A(2^{2\gamma_D} - 1)\sigma_D^2}{2\lambda_D(\boldsymbol{\theta}_D^{**})}, \quad (10)$$

where $\boldsymbol{\theta}_U^{**} \triangleq \arg \max_{\boldsymbol{\theta}_U} \lambda_U(\boldsymbol{\theta}_U)$ and $\boldsymbol{\theta}_D^{**} \triangleq \arg \max_{\boldsymbol{\theta}_D} \lambda_D(\boldsymbol{\theta}_D)$ denote the channel gain maximization (CGM) based beamforming vectors at both IRSs, which are optimal for the HD system. $\lambda_U(\boldsymbol{\theta}_U^{**}) \triangleq |h_{AU} + \mathbf{f}_{AU}^H \boldsymbol{\theta}_U^{**}|^2$ and $\lambda_D(\boldsymbol{\theta}_D^{**}) \triangleq |h_{DA} + \mathbf{g}_{DA}^H \boldsymbol{\theta}_D^{**}|^2$ denote the maximum channel gains for the link between the UL user and the AP and that between the AP and the DL user, respectively. It is readily seen that

$$\boldsymbol{\theta}_U^{**} = \exp(j(\angle h_{AU} \mathbf{1} - \angle \mathbf{f}_{AU})), \quad \boldsymbol{\theta}_D^{**} = \exp(j(\angle h_{DA} \mathbf{1} - \angle \mathbf{g}_{DA})). \quad (11)$$

Based on (9) and (10), we have the following theorem.

Theorem 1. *The minimum power consumption of the FD system is lower than that of the HD system in Case 1, i.e., $\tilde{L}_1(\boldsymbol{\theta}_U^{**}, \boldsymbol{\theta}_D^{**}) \geq L_1(\boldsymbol{\theta}_U^*, \boldsymbol{\theta}_D^*)$, if the following condition is satisfied:*

$$\begin{aligned} \frac{\kappa_A |g|^2}{N^2} \leq U(\boldsymbol{\theta}_U^{**}, \boldsymbol{\theta}_D^{**}) \triangleq & \frac{\kappa_U (|h_{DA}|^2 + |\mathbf{g}_{DA}^H \boldsymbol{\theta}_D^{**}|^2 - 2|h_{DA}| |\mathbf{g}_{DA}^H \boldsymbol{\theta}_D^{**}|) (2^{\gamma_A} - 1)}{6(2^{\gamma_D} - 1)N^2} \\ & + \frac{\kappa_A (|h_{AU}|^2 + |\mathbf{f}_{AU}^H \boldsymbol{\theta}_U^{**}|^2 - 2|h_{AU}| |\mathbf{f}_{AU}^H \boldsymbol{\theta}_U^{**}|) (2^{\gamma_D} - 1) \sigma_D^2}{6(2^{\gamma_A} - 1) \sigma_A^2 N^2} \\ & - \frac{\kappa_A (|\mathbf{f}_{DU}^H \boldsymbol{\theta}_U^{**}|^2 + |\mathbf{g}_{DU}^H \boldsymbol{\theta}_D^{**}|^2)}{N^2}. \end{aligned} \quad (12)$$

Moreover, assuming Rayleigh fading channels for all IRS-related links, i.e., $\mathbf{f}_{IU} \sim \mathcal{CN}(\mathbf{0}, \varrho_{fIU}^2 \mathbf{I})$, $\mathbf{f}_{AI} \sim \mathcal{CN}(\mathbf{0}, \varrho_{fAI}^2 \mathbf{I})$, $\mathbf{g}_{IA} \sim \mathcal{CN}(\mathbf{0}, \varrho_{gIA}^2 \mathbf{I})$, $\mathbf{g}_{DI} \sim \mathcal{CN}(\mathbf{0}, \varrho_{gDI}^2 \mathbf{I})$, $\mathbf{f}_{DI} \sim \mathcal{CN}(\mathbf{0}, \varrho_{fDI}^2 \mathbf{I})$ and $\mathbf{g}_{IU} \sim \mathcal{CN}(\mathbf{0}, \varrho_{gIU}^2 \mathbf{I})$, it holds that when N becomes asymptotically large,

$$U(\boldsymbol{\theta}_U^{**}, \boldsymbol{\theta}_D^{**}) \rightarrow \frac{\kappa_U (2^{\gamma_A} - 1) (1 - \rho)^2 \pi^2 \varrho_{fIU}^2 \varrho_{fAI}^2}{96(2^{\gamma_D} - 1)} + \frac{\bar{\gamma}_2 \pi^2 \varrho_{gIA}^2 \varrho_{gDI}^2 \rho^2}{96(2^{\gamma_A} - 1) \sigma_A^2} > 0. \quad (13)$$

Proof. Please refer to Appendix A. □

Since in (12) $\frac{\kappa_A |g|^2}{N^2} \rightarrow 0$ as $N \rightarrow \infty$, the above condition is always satisfied for sufficiently large N , which implies that with the help of large IRSs, in Case 1 the power consumption of the FD system is asymptotically lower than that of the HD system, regardless of the interference channel gain $|g|^2$. Intuitively, this can be explained by the fact that with sufficiently large IRSs, the interference between the UL user and the DL user can be effectively suppressed, such that FD is ensured to be more spectral efficient than HD.

Remark 1. In contrast, it can be similarly shown that without using IRSs, to guarantee that the power consumption of the FD system is lower than that of the HD system, the following condition must be met:

$$\kappa_A |g|^2 \leq \frac{\kappa_U (2^{\gamma_A} - 1) |h_{DA}|^2}{2(2^{\gamma_D} - 1)} + \frac{\kappa_A (2^{\gamma_D} - 1) |h_{AU}|^2 \sigma_D^2}{2(2^{\gamma_A} - 1) \sigma_A^2}, \quad (14)$$

which, however, does not always hold, especially when the UL-to-DL interference is severe, i.e., when $|g|^2$ is large.

2) *Case 2:* Next, we consider the case of placing all IRS elements to IRS 2 near the DL user. Based on problem (4), the optimal transmit power p_U^* and p_A^* for Case 2 are given by

$$p_U^* = \frac{(2^{\gamma_A} - 1) \sigma_A^2}{|h_{AU}|^2}, \quad (15)$$

$$p_A^* = \frac{(2^{\gamma_D} - 1)\sigma_A^2(2^{\gamma_A} - 1)\omega_{DU}(\boldsymbol{\theta}_{DU})}{|h_{AU}|^2\omega_D(\boldsymbol{\theta}_{DU})} + \frac{(2^{\gamma_D} - 1)\sigma_D^2}{\omega_D(\boldsymbol{\theta}_{DU})}. \quad (16)$$

By defining $\boldsymbol{\theta}_{DU}^*$ as the optimal IRS phase-shift vector for Case 2, the minimum power consumption of the FD system can be expressed as

$$L_2(\boldsymbol{\theta}_{DU}^*) \triangleq \kappa_U p_U^* + \kappa_A p_A^* = \frac{\bar{\gamma}_1 \omega_{DU}(\boldsymbol{\theta}_{DU}^*)}{|h_{AU}|^2 \omega_D(\boldsymbol{\theta}_{DU}^*)} + \frac{\bar{\gamma}_2}{\omega_D(\boldsymbol{\theta}_{DU}^*)} + \frac{\bar{\gamma}_3}{|h_{AU}|^2}. \quad (17)$$

Moreover, similar to (6b) and (6c), the user rate constraints for the corresponding HD system in this case can be expressed as

$$\frac{1}{2} \log \left(1 + \frac{p_U |h_{AU}|^2}{\frac{1}{2} \sigma_A^2} \right) \geq \gamma_A, \quad (18a)$$

$$\frac{1}{2} \log \left(1 + \frac{p_A \omega_D(\boldsymbol{\theta}_{DU})}{\frac{1}{2} \sigma_D^2} \right) \geq \gamma_D. \quad (18b)$$

Then, the minimum power consumption of the HD system in Case 2 can be expressed as

$$\tilde{L}_2(\boldsymbol{\theta}_{DU}^{**}) = \frac{\kappa_U (2^{2\gamma_A} - 1) \sigma_A^2}{2|h_{AU}|^2} + \frac{\kappa_A (2^{2\gamma_D} - 1) \sigma_D^2}{2\omega_D(\boldsymbol{\theta}_{DU}^{**})}, \quad (19)$$

where $\boldsymbol{\theta}_{DU}^{**} \triangleq \arg \max_{\boldsymbol{\theta}_{DU}} \omega_D(\boldsymbol{\theta}_{DU})$ denotes the CGM beamforming vector in this case, which is optimal for the HD system. Similarly, we have

$$\boldsymbol{\theta}_{DU}^{**} = \exp(j(\angle h_{DA} \mathbf{1} - \angle \tilde{\mathbf{g}}_{DA})). \quad (20)$$

The CGM beamforming leads to the channel gains $\omega_D(\boldsymbol{\theta}_{DU}^{**}) \triangleq |h_{DA} + \tilde{\mathbf{g}}_{DA}^H \boldsymbol{\theta}_{DU}^{**}|^2$ and $\omega_{DU}(\boldsymbol{\theta}_{DU}^{**}) \triangleq |g + \tilde{\mathbf{g}}_{DU}^H \boldsymbol{\theta}_{DU}^{**}|^2$ for the link between the AP and the DL user and that between the UL user and the DL user, respectively. By comparing $L_2(\boldsymbol{\theta}_{DU}^*)$ and $\tilde{L}_2(\boldsymbol{\theta}_{DU}^{**})$, we obtain the following theorem.

Theorem 2. *The minimum power consumption of the FD system is lower than that of the HD system in Case 2, if the following condition is satisfied:*

$$\begin{aligned} \frac{\kappa_A |g|^2}{N^2} \leq U(\boldsymbol{\theta}_{DU}^{**}) \triangleq & \frac{\kappa_U (2^{\gamma_A} - 1) (|h_{DA}|^2 + |\tilde{\mathbf{g}}_{DA}^H \boldsymbol{\theta}_{DU}^{**}|^2 - 2|h_{DA}| |\tilde{\mathbf{g}}_{DA}^H \boldsymbol{\theta}_{DU}^{**}|)}{4(2^{\gamma_D} - 1)N^2} \\ & + \frac{\kappa_A (2^{\gamma_D} - 1) |h_{AU}|^2 \sigma_D^2}{4(2^{\gamma_A} - 1) \sigma_A^2 N^2} - \frac{\kappa_A |\tilde{\mathbf{g}}_{DU}^H \boldsymbol{\theta}_{DU}^{**}|^2}{N^2}. \end{aligned} \quad (21)$$

Assuming Rayleigh fading channels for all IRS-related links, i.e., $\tilde{\mathbf{g}}_{IA} \sim \mathcal{CN}(\mathbf{0}, \varrho_{g_{IA}}^2 \mathbf{I})$, $\tilde{\mathbf{g}}_{DI} \sim \mathcal{CN}(\mathbf{0}, \varrho_{g_{DI}}^2 \mathbf{I})$ and $\tilde{\mathbf{g}}_{IU} \sim \mathcal{CN}(\mathbf{0}, \varrho_{g_{IU}}^2 \mathbf{I})$, it follows that when N becomes asymptotically large,

$$U(\boldsymbol{\theta}_{DU}^{**}) \rightarrow \frac{\kappa_U (2^{\gamma_A} - 1) (16|h_{DA}|^2 + \pi^2 \varrho_{g_{IA}}^2 \varrho_{g_{DI}}^2)}{64(2^{\gamma_D} - 1)} > 0. \quad (22)$$

Proof. Please refer to Appendix B. \square

From the above, we see that with sufficiently large N , in Case 2 the FD system always outperforms the HD system, regardless of the interference channel gain $|g|^2$.

3) *Case 3*: Last, for the case of placing all reflecting elements to IRS 1 near the UL user, the minimum power consumption of the FD system can be expressed as

$$L_3(\tilde{\boldsymbol{\theta}}_{DU}^*) \triangleq \frac{\bar{\gamma}_1 \xi_{DU}(\tilde{\boldsymbol{\theta}}_{DU}^*)}{|h_{DA}|^2 \xi_U(\tilde{\boldsymbol{\theta}}_{DU}^*)} + \frac{\bar{\gamma}_3}{\xi_U(\tilde{\boldsymbol{\theta}}_{DU}^*)} + \frac{\bar{\gamma}_2}{|h_{DA}|^2}, \quad (23)$$

where $\tilde{\boldsymbol{\theta}}_{DU}^*$ denotes the optimal IRS phase-shift vector for Case 3. By following the same approach for Case 2, we can obtain the same conclusion for the FD system in Case 3 when N becomes sufficiently large. Hence, we omit the details for brevity.

B. Comparison of Different IRS Deployment Cases

In the following, we focus on the FD system and compare the minimum power consumption among Case 1, Case 2 and Case 3 to find which deployment strategy performs the best. In particular, we derive an asymptotic result when the number of reflecting elements N becomes large.

With the minimum power consumption in Case 1 expressed in (9), we provide the following theorem.

Theorem 3. *Assuming Rayleigh fading channels for all IRS-related links, the upper bound of the minimum power consumption of the FD system in Case 1 quadratically decreases to 0 with the increasing of N .*

Proof. Please refer to Appendix C. □

Besides, we can rewrite the expressions of the minimum power consumption of the FD system in (17) and (23) for Case 2 and Case 3 as follows:

$$L_2(\boldsymbol{\theta}_{DU}^*) = \frac{\bar{\gamma}_1 \omega_{DU}(\boldsymbol{\theta}_{DU}^*)}{|h_{AU}|^2 \omega_D(\boldsymbol{\theta}_{DU}^*)} + \frac{\bar{\gamma}_2}{\omega_D(\boldsymbol{\theta}_{DU}^*)} + \frac{\bar{\gamma}_3}{|h_{AU}|^2} > \frac{\bar{\gamma}_3}{|h_{AU}|^2} > 0, \quad (24)$$

$$L_3(\tilde{\boldsymbol{\theta}}_{DU}^*) = \frac{\bar{\gamma}_1 \xi_{DU}(\tilde{\boldsymbol{\theta}}_{DU}^*)}{|h_{DA}|^2 \xi_U(\tilde{\boldsymbol{\theta}}_{DU}^*)} + \frac{\bar{\gamma}_3}{\xi_U(\tilde{\boldsymbol{\theta}}_{DU}^*)} + \frac{\bar{\gamma}_2}{|h_{DA}|^2} > \frac{\bar{\gamma}_2}{|h_{DA}|^2} > 0. \quad (25)$$

It is observed from (24) and (25) that $L_2(\boldsymbol{\theta}_{DU}^*)$ and $L_3(\tilde{\boldsymbol{\theta}}_{DU}^*)$ are lower-bounded by $\frac{\bar{\gamma}_3}{|h_{AU}|^2}$ and $\frac{\bar{\gamma}_2}{|h_{DA}|^2}$, respectively. Based on (24), (25) and Theorem 3, we can conclude that with sufficiently large N , the minimum power consumption in Case 1 is much lower than that in either Case 2 or 3, which means that the distributed deployment generally outperforms the centralized deployment in terms of power consumption. The reason is that, when $N \rightarrow \infty$, in Case 1 both users have asymptotically large channel gains and the DL user has diminishing interference, whereas Case 2 and Case 3 cannot achieve all the above at the same time.

IV. PASSIVE BEAMFORMING OPTIMIZATION

In this section, we propose a new BCD-based algorithm to optimize the passive beamforming vector at the IRSs, for a general channel model and an arbitrary value of N . Subsequently, we discuss the convergence and computational complexity of the proposed algorithm.

A. BCD-Based Passive Beamforming Design

Let us first focus on Case 1 to introduce the proposed algorithm in general (as Cases 2 and 3 are special cases of Case 1). By substituting the optimal transmit powers in (7) and (8) into the original optimization problem (3), we have the following equivalent problem:

$$\min_{\phi_U, \phi_D} \frac{\bar{\gamma}_1 |g + \mathbf{f}_{DU}^H \boldsymbol{\psi}_U + \mathbf{g}_{DU}^H \boldsymbol{\psi}_D|^2}{|h_{DA} + \mathbf{g}_{DA}^H \boldsymbol{\psi}_D|^2 |h_{AU} + \mathbf{f}_{AU}^H \boldsymbol{\psi}_U|^2} + \frac{\bar{\gamma}_2}{|h_{DA} + \mathbf{g}_{DA}^H \boldsymbol{\psi}_D|^2} + \frac{\bar{\gamma}_3}{|h_{AU} + \mathbf{f}_{AU}^H \boldsymbol{\psi}_U|^2}, \quad (26)$$

where $\boldsymbol{\psi}_U \triangleq \exp(j\phi_U)$, $\boldsymbol{\psi}_D \triangleq \exp(j\phi_D)$, $\phi_U \triangleq \angle \boldsymbol{\theta}_U$ and $\phi_D \triangleq \angle \boldsymbol{\theta}_D$. Note that in (26), the phase-shift values (i.e., ϕ_U and ϕ_D) of the IRS reflection coefficients are regarded as the optimization variables and $\{\boldsymbol{\psi}_U, \boldsymbol{\psi}_D\}$ are treated as functions of these phase-shift values, thus the original uni-modular constraint (3d) in problem (3) can be safely ignored.

Problem (26) is still difficult to solve due to the fractional coupling terms in the objective function. In this paper, we first transform (26) into an equivalent but more tractable form and then develop a BCD-based algorithm to solve the equivalent problem. By reducing the fractions of the objective function in (26) to a common denominator and taking the reciprocal, we obtain an equivalent expression of problem (26) as

$$\max_{\phi_U, \phi_D} \frac{|h_{DA} + \mathbf{g}_{DA}^H \boldsymbol{\psi}_D|^2 |h_{AU} + \mathbf{f}_{AU}^H \boldsymbol{\psi}_U|^2}{\bar{\gamma}_1 |g + \mathbf{f}_{DU}^H \boldsymbol{\psi}_U + \mathbf{g}_{DU}^H \boldsymbol{\psi}_D|^2 + \bar{\gamma}_2 |h_{AU} + \mathbf{f}_{AU}^H \boldsymbol{\psi}_U|^2 + \bar{\gamma}_3 |h_{DA} + \mathbf{g}_{DA}^H \boldsymbol{\psi}_D|^2}. \quad (27)$$

Then, we can state the following theorem.

Theorem 4. *By introducing an auxiliary variable $v \in \mathbb{R}$, problem (27) can be equivalently formulated as the following problem in the sense that both problems share the same global optimal solutions for ϕ_U and ϕ_D :*

$$\min_{v, \phi_U, \phi_D} v^2 (\bar{\gamma}_1 |g + \mathbf{f}_{DU}^H \boldsymbol{\psi}_U + \mathbf{g}_{DU}^H \boldsymbol{\psi}_D|^2 + \bar{\gamma}_2 |h_{AU} + \mathbf{f}_{AU}^H \boldsymbol{\psi}_U|^2 + \bar{\gamma}_3 |h_{DA} + \mathbf{g}_{DA}^H \boldsymbol{\psi}_D|^2) - 2\Re(\text{conj}(v)(h_{DA} + \mathbf{g}_{DA}^H \boldsymbol{\psi}_D)(h_{AU} + \mathbf{f}_{AU}^H \boldsymbol{\psi}_U)). \quad (28)$$

Proof. Please refer to Appendix D. □

Problem (28) can be solved based on the BCD method, where we partition the variables into multiple blocks which are updated sequentially in each iteration. To this end, the variables are

updated as follows: 1) update v by fixing the other variables; 2) update $\phi_U(n), \forall n$, sequentially with the other variables fixed; 3) update $\phi_D(n), \forall n$, sequentially with the other variables fixed. The detailed updating procedure is presented as follows.

In **Step 1**, we optimize v by fixing the other variables. The subproblem for v is given by

$$\min_v v^2 a - 2\Re(\text{conj}(v)b), \quad (29)$$

where $a = \bar{\gamma}_1|g + \mathbf{f}_{DU}^H \boldsymbol{\psi}_U + \mathbf{g}_{DU}^H \boldsymbol{\psi}_D|^2 + \bar{\gamma}_2|h_{AU} + \mathbf{f}_{AU}^H \boldsymbol{\psi}_U|^2 + \bar{\gamma}_3|h_{DA} + \mathbf{g}_{DA}^H \boldsymbol{\psi}_D|^2$ and $b = (h_{DA} + \mathbf{g}_{DA}^H \boldsymbol{\psi}_D)(h_{AU} + \mathbf{f}_{AU}^H \boldsymbol{\psi}_U)$. We can obtain the optimal solution of this subproblem as $v^* = \frac{b}{a}$ by checking the first order optimality condition.

In **Step 2**, we optimize $\phi_U(n), \forall n$, sequentially by fixing the other variables. The corresponding subproblem for $\phi_U(n)$ is given by

$$\begin{aligned} \min_{\phi_U(n)} v^2 (\bar{\gamma}_1|g + \mathbf{f}_{DU}^H \boldsymbol{\psi}_U + \mathbf{g}_{DU}^H \boldsymbol{\psi}_D|^2 + \bar{\gamma}_2|h_{AU} + \mathbf{f}_{AU}^H \boldsymbol{\psi}_U|^2) \\ - 2\Re(\text{conj}(v)(h_{DA} + \mathbf{g}_{DA}^H \boldsymbol{\psi}_D)(h_{AU} + \mathbf{f}_{AU}^H \boldsymbol{\psi}_U)). \end{aligned} \quad (30)$$

By appropriately rearranging the objective function of problem (30), we have the following equivalent problem:

$$\min_{\phi_U(n)} \boldsymbol{\psi}_U^H \mathbf{A}_{\psi_U} \boldsymbol{\psi}_U - 2\Re(\boldsymbol{\psi}_U^H \mathbf{b}_{\psi_U}), \quad (31)$$

where $\mathbf{A}_{\psi_U} \triangleq |v|^2(\bar{\gamma}_1 \mathbf{f}_{DU} \mathbf{f}_{DU}^H + \bar{\gamma}_2 \mathbf{f}_{AU} \mathbf{f}_{AU}^H)$ and $\mathbf{b}_{\psi_U} \triangleq v(\text{conj}(h_{DA}) + \phi_D^H \mathbf{g}_{DA}) \mathbf{f}_{AU} - |v|^2(\bar{\gamma}_1 \mathbf{f}_{DU}(g + \mathbf{g}_{DU}^H \phi_D) + \bar{\gamma}_2 \mathbf{f}_{AU} h_{AU})$. It is readily seen that the objective function of problem (31) is a quadratic function with respect to $\boldsymbol{\psi}_U(n)$. Hence, by omitting the irrelevant constant terms, we can rewrite problem (31) as follows:

$$\min_{\phi_U(n)} \bar{a}_{\psi_U, n} |\boldsymbol{\psi}_U(n)|^2 - 2\Re(\text{conj}(\bar{b}_{\psi_U, n}) \boldsymbol{\psi}_U(n)), \quad (32)$$

where $\bar{a}_{\psi_U, n}$ is a known coefficient that is not related to $\phi_U(n)$, $\bar{b}_{\psi_U, n} = \mathbf{A}_{\psi_U}(n, n) \boldsymbol{\psi}_U(n) - \mathbf{A}_{\psi_U}(n, :) \boldsymbol{\psi}_U + \mathbf{b}_{\psi_U}(n)$, and $\mathbf{A}_{\psi_U}(n, :)$ denotes the n th row vector of matrix \mathbf{A}_{ψ_U} . Obviously, the optimal solution of problem (32) is given by $\phi_U^*(n) = \angle \bar{b}_{\psi_U, n}$.

In **Step 3**, we optimize $\phi_D(n), \forall n$, sequentially by fixing the other variables. The corresponding subproblem is given by

$$\begin{aligned} \min_{\phi_D(n)} v^2 (\bar{\gamma}_1|g + \mathbf{f}_{DU}^H \boldsymbol{\psi}_U + \mathbf{g}_{DU}^H \boldsymbol{\psi}_D|^2 + \bar{\gamma}_3|h_{DA} + \mathbf{g}_{DA}^H \boldsymbol{\psi}_D|^2) \\ - 2\Re(\text{conj}(v(h_{DA} + \mathbf{g}_{DA}^H \boldsymbol{\psi}_D)(h_{AU} + \mathbf{f}_{AU}^H \boldsymbol{\psi}_U))). \end{aligned} \quad (33)$$

This subproblem can be similarly solved as problem (30), thus the details are omitted for brevity.

In summary, we can solve problem (26) by iterating over the abovementioned three steps and the overall BCD-based algorithm is summarized in Algorithm 1.

Algorithm 1 Proposed BCD-based passive beamforming design algorithm

1. Define the tolerance of accuracy δ . Initialize the algorithm with a feasible point. Set the iteration number $i = 0$ and the maximum iteration number N_{\max} .
 2. **Repeat**
 - Update v , $\phi_U(n)$, $\forall n$ and $\phi_D(n)$, $\forall n$ sequentially according to **Steps** 1-3, respectively.
 - Update the iteration number : $i \leftarrow i + 1$.
 3. **Until** the fractional decrease of (28) is less than δ or the maximum number of iterations is reached, i.e., $i > N_{\max}$.
-

Besides, the passive beamforming optimization problems for Case 2 and Case 3 can be written as

$$\min_{\phi_{DU}} \frac{\bar{\gamma}_1 |g + \tilde{\mathbf{g}}_{DU}^H \boldsymbol{\psi}_{DU}|^2}{|h_{AU}|^2 |h_{DA} + \tilde{\mathbf{g}}_{DA}^H \boldsymbol{\psi}_{DU}|^2} + \frac{\bar{\gamma}_2}{|h_{DA} + \tilde{\mathbf{g}}_{DA}^H \boldsymbol{\psi}_{DU}|^2}, \quad (34)$$

$$\min_{\tilde{\phi}_{DU}} \frac{\bar{\gamma}_1 |g + \tilde{\mathbf{f}}_{DU}^H \tilde{\boldsymbol{\psi}}_{DU}|^2}{|h_{DA}|^2 |h_{AU} + \tilde{\mathbf{f}}_{AU}^H \tilde{\boldsymbol{\psi}}_{DU}|^2} + \frac{\bar{\gamma}_3}{|h_{AU} + \tilde{\mathbf{f}}_{AU}^H \tilde{\boldsymbol{\psi}}_{DU}|^2}, \quad (35)$$

respectively, where $\boldsymbol{\psi}_{DU} \triangleq \exp(j\phi_{DU})$, $\phi_{DU} \triangleq \angle \boldsymbol{\theta}_{DU}$, $\tilde{\boldsymbol{\psi}}_{DU} \triangleq \exp(j\tilde{\phi}_{DU})$ and $\tilde{\phi}_{DU} \triangleq \angle \tilde{\boldsymbol{\theta}}_{DU}$. Since Algorithm 1 can be easily modified to solve problems (34) and (35) as well, the details are omitted here.

B. Complexity and Convergence of Algorithm 1

The complexity of Algorithm 1 is dominated by the matrix multiplication operations required for updating ϕ_U and ϕ_D . Thus, by omitting the lower order terms, the overall complexity of Algorithm 1 is given by $\mathcal{O}(IN^2)$, where I is the iteration number required by Algorithm 1.

As for the convergence property of Algorithm 1, it is seen that each subproblem in the proposed BCD-based algorithm is globally and uniquely solved. Therefore, according to Proposition 2.7.1 (Convergence of Block Coordinate Descent) in [35], Algorithm 1 is guaranteed to converge to a Karush–Kuhn–Tucker (KKT) point of problem (28), i.e., a solution satisfying the KKT conditions of the problem. Furthermore, according to [36], problem (28) and problem (27) share the same KKT points. Therefore, Algorithm 1 is guaranteed to converge to a KKT point of problem (27), which is also a KKT point of problem (26).

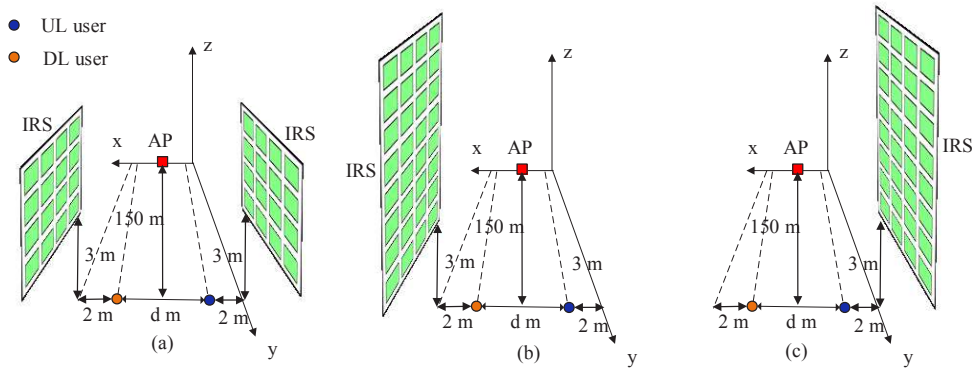


Fig. 2: Simulation setup. (a) Case 1: Place IRSs on both user sides; (b) Case 2: IRS is placed near the DL user only; (c) Case 3: IRS is placed near the UL user only.

V. SIMULATION RESULTS

In this section, we validate our analysis and evaluate the performance of the proposed algorithm based on simulations. The path loss is modeled as $L = C_0(d_{\text{link}}/D_0)^{-\alpha}$, where C_0 is the path loss at the reference distance of $D_0 = 1$ m, α is the path-loss exponent and d_{link} represents the link distance. We denote the path-loss exponents of the AP-user (both UL and DL), AP-IRS, IRS-user and user-user links as α_{DA} , α_{IA} , α_{DI} and α_{DU} , respectively, and set $\alpha_{DA} = 3.6$ and $\alpha_{IA} = \alpha_{DI} = \alpha_{DU} = 2.2$. In the simulations, we construct a 3-D coordinate system where the AP is located on the x -axis and the IRSs are placed in the planes parallel to the $y-z$ plane, as illustrated in Fig. 2. The distance between the UL user and the DL user is represented by d . The reference antenna at AP is located at $(2 + \frac{d}{2}, 0, 0)$, the UL user is located at $(2, 150, 0)$, and the DL user is located at $(d + 2, 150, 0)$. For Case 1, the reference reflecting elements at the two IRSs are placed at $(0, 150, 3)$ m and $(d + 4, 150, 3)$ m, respectively. For Case 2 and Case 3, the reference reflecting element at the combined IRS is placed at $(d + 4, 150, 3)$ m and $(0, 150, 3)$ m, respectively. Besides, we assume the Rician fading channel model for all links in our simulations since both line-of-sight (LoS) and non-LoS (NLoS) components may exist in practical channels. Accordingly, the AP-IRS and IRS-user channels are modeled as

$$\mathbf{f} = \sqrt{\frac{\beta}{1 + \beta}} \mathbf{f}^{\text{LoS}} + \sqrt{\frac{1}{1 + \beta}} \mathbf{f}^{\text{NLoS}}, \quad (36)$$

where β is the Rician factor, \mathbf{f}^{LoS} and \mathbf{f}^{NLoS} denote the deterministic LoS and NLoS components, respectively. Here we denote the Rician factors of the AP-IRS and IRS-user links as β_{IA} and β_{DI} , respectively, and we set $\beta_{IA} = 9$ dB and $\beta_{DI} = 6$ dB in our simulations. g is modeled

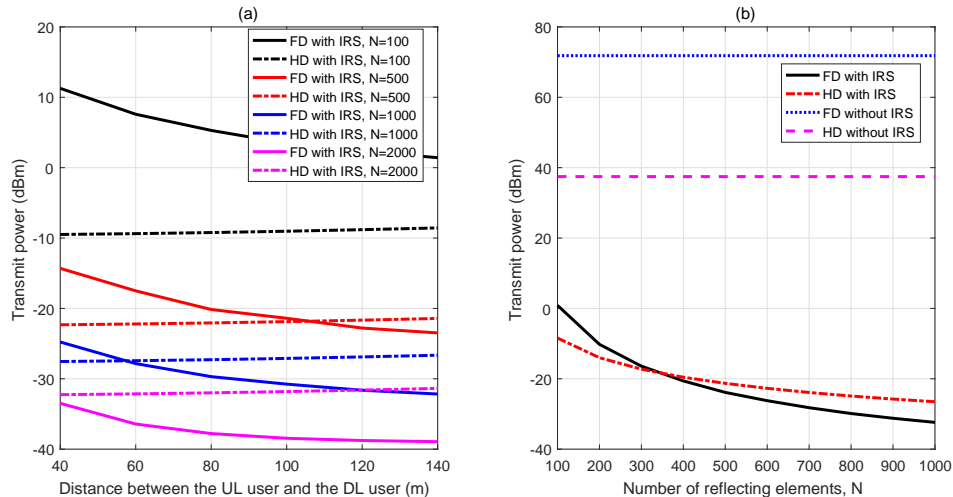


Fig. 3: Minimum power consumption in Case 1: (a) Transmit power versus the distance between the UL and DL users; (b) Transmit power versus the total number of IRS reflecting elements.

similarly, with the Rician factor equal to 4 dB. Without loss of generality, we set $\rho = 0.5$ and $\kappa_U = \kappa_A = 1$ in all of our simulations.

In the following, we first show the advantage of using IRS over without using IRS by comparing the minimum transmit power required in the FD and HD systems under different IRS deployment strategies. Then, we compare the performance of the three IRS deployment strategies based on the FD system.

A. FD versus HD Systems

In this subsection, we aim to verify our analytical results in Section III-A by simulations. Thus, the IRS reflection coefficients for the considered three deployment strategies are set based on the CGM beamforming given in Section III to maximize the channel power gains of the IRS-related links. Unless otherwise specified, we set $d = 80$ m and $\gamma_A = \gamma_D = 4$ bits/s/Hz.

First, consider the performance comparison between the FD and HD systems in Case 1. Fig. 3 shows the minimum total transmit power consumption (for both the AP and UL user) versus the distance between the UL and DL users, d , as well as the total number of IRS reflecting elements, N . From Fig. 3 (a), we can see that the power consumption of the FD system decreases with the increasing of d while the power consumption of the HD system gradually increases with the increasing of d . This is because the UL-to-DL interference in general weakens as d increases, which is beneficial for improving the performance of the FD system; on the other

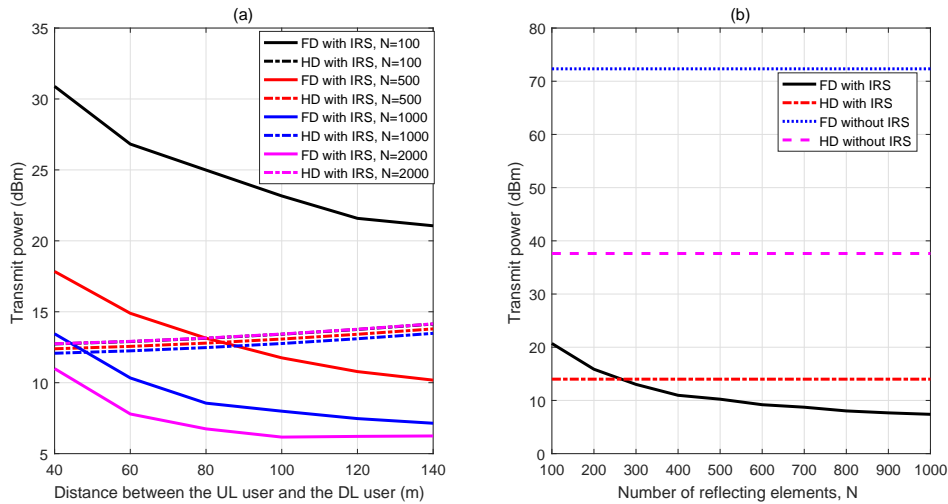


Fig. 4: Minimum power consumption in Case 2: (a) Transmit power versus the distance between the UL and DL users; (b) Transmit power versus the total number of IRS reflecting elements.

hand, larger d implies longer distance between the AP and users and more severe path losses of the AP-user links, therefore although there is no UL-to-DL interference in the HD system, its performance could be impaired as d increases. Moreover, it is observed that the transmit powers of all considered systems decrease with the increasing of N , which is expected since larger N leads to higher passive beamforming gain. Fig. 3 (b) illustrates the relationship between the transmit power and the number of reflecting elements at the IRSs for both FD and HD systems. From the results, we can see that the transmit power of the FD system is larger than that of the HD system when there is no IRS or N is small; however the transmit power of the FD system becomes much smaller than that of the HD system with the increasing of N , which verifies the results in Theorem 1.

Then, we compare the transmit power consumption in the FD and HD systems for Case 2 and Case 3. Fig. 4 (a) and (b) illustrate the transmit power performance versus the distance d and the number of IRS reflecting elements in Case 2, respectively, and the same comparison is shown in Fig. 5 (a) and (b) for Case 3. Similar to Case 1, from Fig. 4 (a) and Fig. 5 (a), the transmit power of the FD system decreases while that of the HD system slightly increases with d in both Case 2 and Case 3. The reason for this phenomenon is the same as the aforementioned one for Case 1. In Fig. 4 (b) and Fig. 5 (b), the trend of the curves regarding the HD system with IRS does not decrease much with the increasing number of reflecting elements, which is different from its counterpart in Case 1. This can be explained by the fact that with only one large IRS deployed

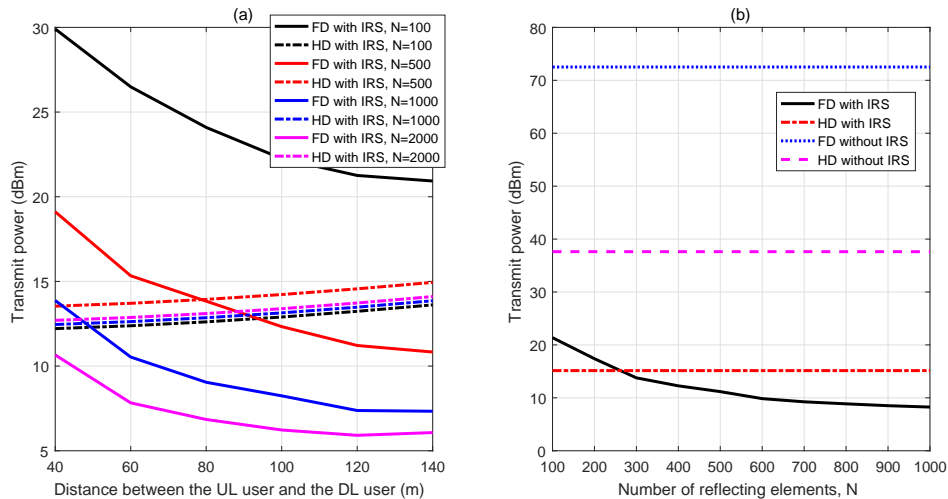


Fig. 5: Minimum power consumption in Case 3: (a) Transmit power versus the distance between the UL and DL users; (b) Transmit power versus the total number of IRS reflecting elements.

near the DL (or UL) user, the power consumption required for achieving the rate requirement of the UL (DL) user cannot be reduced, thus the total transmit power consumption in Case 2 (Case 3) is dominated by the power required by the UL (DL) transmission which remains unchanged under different values of N . From the above results, we can see that the FD and HD systems with IRS achieve much lower transmit power consumption as compared to those without IRS. Furthermore, the transmit power of the FD system becomes much smaller than that of the HD system with the increasing of N . The results thus verify the discussions in Section III-A for Cases 2 and 3.

B. Comparison of Different IRS Deployment Strategies in FD System

In this subsection, we evaluate the performance of our proposed BCD-based passive beamforming algorithm (i.e., Algorithm 1) in the FD system and compare the performance of different IRS deployment strategies. Unless otherwise specified, we assume $\gamma_A = \gamma_D = 4$ bits/s/Hz, $N = 2000$ and $d = 40$ m for all cases.

We first investigate the convergence behavior of our proposed BCD-based algorithm. Fig. 6 shows the achieved objective value versus the number of iterations in Case 1. The phase shifts are randomly initialized within $[0, 2\pi)$. It is observed that the transmit power achieved by the proposed algorithm decreases monotonically with the number of iterations and the proposed algorithm can converge within 60 iterations. Moreover, the proposed algorithm has a low com-

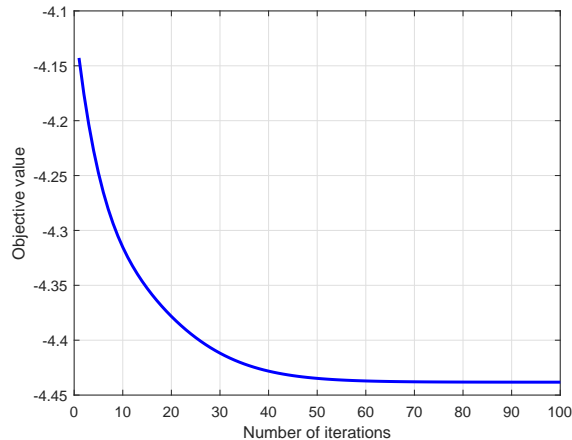


Fig. 6: Convergence behavior of the proposed BCD-based passive beamforming algorithm.

plexity due to the closed-form solution (multiplication operation only) of each step shown in Algorithm 1.

Next, we study in Fig. 7 the effect of the rate requirement of the UL user, i.e., γ_A , on the transmit power consumption, under the three IRS deployment strategies. We can see from this figure that the transmit power of Case 1 is significantly lower than that of Case 2 or Case 3, which shows the advantage of distributed deployment over centralized deployment under the considered FD system. Besides, we observe that the transmit power in Case 3 increases slower than that in Case 2 with the increase of γ_A . This is because in Case 3, the IRS is placed near the UL user and thus the rate requirement of the UL user can be met easier. Moreover, we can see that the proposed BCD-based passive beamforming algorithm achieves better performance compared to the CGM passive beamforming algorithm, especially when γ_A is large. This is mainly because the UL-to-DL interference becomes the performance bottleneck in the high- γ_A regime and simply employing the CGM based beamforming cannot effectively suppress this interference. Similarly, we explore in Fig. 8 the effect of the rate requirement of the DL user, i.e., γ_D , on the transmit power consumption. We can see that Case 1 also outperforms Case 2 and Case 3 under this setup. Besides, the transmit power in Case 2 increases slower than that in Case 3 as γ_D increases since the rate requirement of the DL user can be more easily satisfied in this case.

Finally, in Fig. 9, we investigate the effect of the number of IRS reflecting elements on the transmit power performance for the three IRS deployment strategies. It can be seen that the performance of Case 1 is the best among all considered. Besides, the distributed deployment

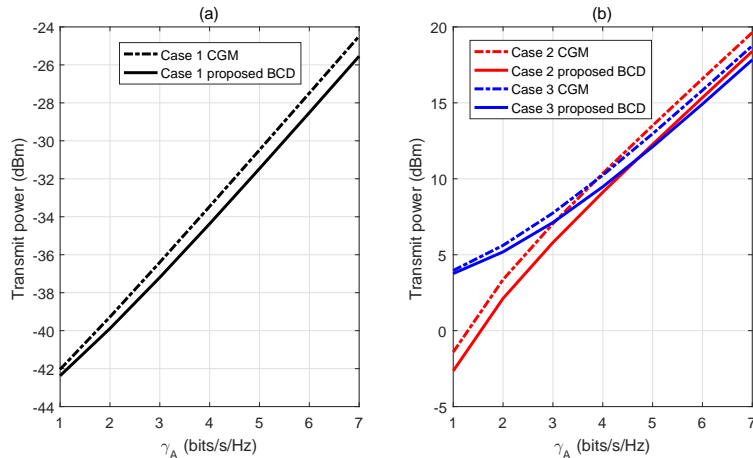


Fig. 7: Transmit power versus γ_A for the proposed BCD-based algorithm and the CGM algorithm: (a) Case 1; (b) Case 2 and Case 3.

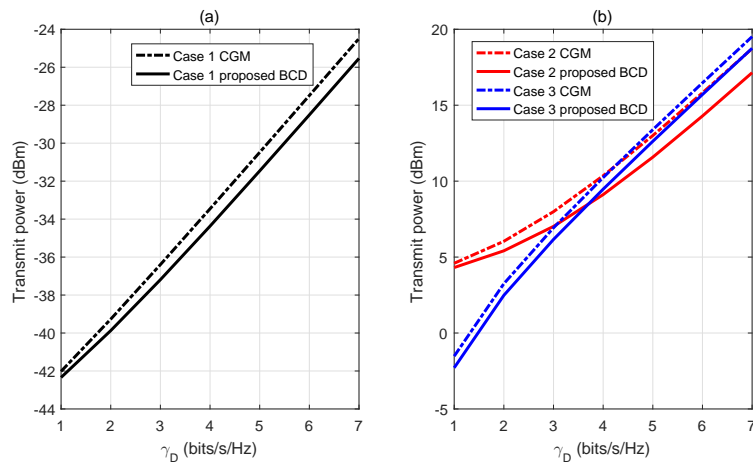


Fig. 8: Transmit power versus γ_D for the proposed BCD-based algorithm and the CGM algorithm: (a) Case 1; (b) Case 2 and Case 3.

strategy in Case 1 also provides the largest performance improvement when N is increased from 400 to 2000, e.g., the transmit power when $N = 2000$ is about 20 dBm lower than that when $N = 400$ in Case 1, but this gain is only around 10 dBm in Cases 2 and 3. These results coincide with the analysis in Section III-B. Furthermore, we can see that the proposed BCD-based algorithm still outperforms the CGM algorithm and the gain increases with the number of reflecting elements. This is because larger N offers more flexibility when designing the reflection coefficients and a more significant tradeoff between channel gain and UL-to-DL interference can be achieved by the proposed BCD-based algorithm, while only channel gain maximization is

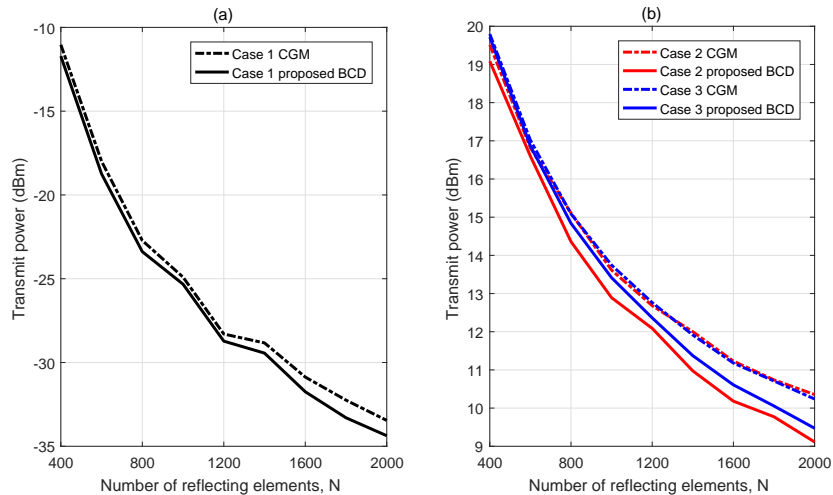


Fig. 9: Transmit power versus the number of IRS reflecting elements for the proposed BCD-based algorithm and the CGM algorithm: (a) Case 1; (b) Case 2 and Case 3.

considered in the CGM algorithm.

VI. CONCLUSIONS AND FUTURE WORK

In this paper, we have studied three deployment cases for an IRS-aided FD wireless system. In each case, the weighted sum transmit power consumption of the AP and UL user is minimized by jointly optimizing their transmit power and the passive reflection coefficients at the IRS (or IRSs), subject to the UL and DL users' rate constraints and the uni-modulus constraints on the IRS reflection coefficients. We have analyzed the minimum transmit power in the IRS-aided FD system under the three deployment schemes, as compared with that of the corresponding HD system. Specifically, we have showed that the FD system outperforms its HD counterpart for all IRS deployment schemes, while the distributed deployment further outperforms the other two centralized deployment schemes. Moreover, we have developed an efficient BCD-based algorithm for passive beamforming design in a general system setup. Finally, numerical results have been presented to verify our analysis and the efficacy of the proposed passive beamforming design algorithm.

In the following, we briefly discuss some important issues/aspects of this work that are not addressed yet, so as to motivate future research.

- For simplicity, we only considered the single UL/DL user case and the two users are assumed to be equipped with a single antenna each. Besides, the FD AP is also assumed to have a

single transmit/receive antenna. Generally, there may exist multiple UL/DL users, and the AP as well as users are usually equipped with multiple antennas for high-rate communications, therefore the joint design of active beamforming at the AP/users and passive beamforming at the IRS is an important problem to investigate in the future.

- In this paper, we considered continuous phase shifts at the reflecting elements of the IRS, which may be practically difficult to implement due to the hardware limitation. Besides, the reflection amplitudes at the IRS were assumed to be 1 for simplicity and the potential joint optimization of reflection amplitudes and phase shifts [37] was not exploited. Thus, beamforming optimization with discrete phase shifts at the IRS and joint reflection amplitude and phase-shift optimization are interesting topics, which are worthy of further investigation.
- In practice, the SI due to the FD operation cannot be perfectly canceled in general and CSI errors are inevitable in practice due to limited channel training resources. Therefore, beamforming optimization under more practice channel model is also an important problem to investigate in future work.

APPENDIX A

PROOF FOR THEOREM 1

By comparing $L_1(\boldsymbol{\theta}_U^*, \boldsymbol{\theta}_D^*)$ and $\tilde{L}_1(\boldsymbol{\theta}_U^{**}, \boldsymbol{\theta}_D^{**})$, we obtain

$$\begin{aligned}
& \tilde{L}_1(\boldsymbol{\theta}_U^{**}, \boldsymbol{\theta}_D^{**}) - L_1(\boldsymbol{\theta}_U^*, \boldsymbol{\theta}_D^*) \\
&= \frac{\kappa_U(2^{\gamma_A} + 1)(2^{\gamma_A} - 1)\sigma_A^2}{2\lambda_U(\boldsymbol{\theta}_U^{**})} + \frac{\kappa_A(2^{\gamma_D} + 1)(2^{\gamma_D} - 1)\sigma_D^2}{2\lambda_D(\boldsymbol{\theta}_D^{**})} \\
&\quad - \left(\frac{\bar{\gamma}_3}{\lambda_U(\boldsymbol{\theta}_U^*)} + \frac{\bar{\gamma}_2}{\lambda_D(\boldsymbol{\theta}_D^*)} + \frac{\bar{\gamma}_1\lambda_{DU}(\boldsymbol{\theta}_U^*, \boldsymbol{\theta}_D^*)}{\lambda_D(\boldsymbol{\theta}_D^*)\lambda_U(\boldsymbol{\theta}_U^*)} \right) \\
&\geq \tilde{L}_1(\boldsymbol{\theta}_U^{**}, \boldsymbol{\theta}_D^{**}) - L_1(\boldsymbol{\theta}_U^{**}, \boldsymbol{\theta}_D^{**}) \\
&= \frac{\kappa_U(2^{\gamma_A} - 1)^2\sigma_A^2}{2\lambda_U(\boldsymbol{\theta}_U^{**})} + \frac{\kappa_A(2^{\gamma_D} - 1)^2\sigma_D^2}{2\lambda_D(\boldsymbol{\theta}_D^{**})} - \frac{\bar{\gamma}_1\lambda_{DU}(\boldsymbol{\theta}_U^{**}, \boldsymbol{\theta}_D^{**})}{\lambda_D(\boldsymbol{\theta}_D^{**})\lambda_U(\boldsymbol{\theta}_U^{**})},
\end{aligned} \tag{37}$$

where $\lambda_{DU}(\boldsymbol{\theta}_U^{**}, \boldsymbol{\theta}_D^{**}) \triangleq |g + \mathbf{f}_{DU}^H \boldsymbol{\theta}_U^{**} + \mathbf{g}_{DU}^H \boldsymbol{\theta}_D^{**}|^2$ denotes the channel power gain between the UL user and the DL user with the CGM beamforming and the inequality holds since the CGM beamforming vectors $\boldsymbol{\theta}_U^{**}$ and $\boldsymbol{\theta}_D^{**}$ shown in (11) are suboptimal solutions of problem (3) in general and $L_1(\boldsymbol{\theta}_U^{**}, \boldsymbol{\theta}_D^{**}) \geq L_1(\boldsymbol{\theta}_U^*, \boldsymbol{\theta}_D^*)$. Note that in light of the Cauchy-Schwarz inequality²,

²Our result also holds by the fact that for two complex numbers x and y , the following inequality holds $||x| - |y|| \leq |x + y| \leq |x| + |y|$.

we can obtain

$$\lambda_{DU}(\boldsymbol{\theta}_U^{**}, \boldsymbol{\theta}_D^{**}) \leq (|g| + |\mathbf{f}_{DU}^H \boldsymbol{\theta}_U^{**}| + |\mathbf{g}_{DU}^H \boldsymbol{\theta}_D^{**}|)^2 \leq 3(|g|^2 + |\mathbf{f}_{DU}^H \boldsymbol{\theta}_U^{**}|^2 + |\mathbf{g}_{DU}^H \boldsymbol{\theta}_D^{**}|^2). \quad (38)$$

Thus, we further have

$$\begin{aligned} & \tilde{L}_1(\boldsymbol{\theta}_U^{**}, \boldsymbol{\theta}_D^{**}) - L_1(\boldsymbol{\theta}_U^*, \boldsymbol{\theta}_D^*) \\ & \geq \frac{\kappa_U(2^{\gamma_A} - 1)^2 \sigma_A^2}{2\lambda_U(\boldsymbol{\theta}_U^{**})} + \frac{\kappa_A(2^{\gamma_D} - 1)^2 \sigma_D^2}{2\lambda_D(\boldsymbol{\theta}_D^{**})} - \frac{3\bar{\gamma}_1(|g|^2 + |\mathbf{f}_{DU}^H \boldsymbol{\theta}_U^{**}|^2 + |\mathbf{g}_{DU}^H \boldsymbol{\theta}_D^{**}|^2)}{\lambda_D(\boldsymbol{\theta}_D^{**})\lambda_U(\boldsymbol{\theta}_U^{**})}. \end{aligned} \quad (39)$$

By multiplying $\frac{\lambda_D(\boldsymbol{\theta}_D^{**})\lambda_U(\boldsymbol{\theta}_U^{**})}{3(2^{\gamma_D}-1)\sigma_A^2(2^{\gamma_A}-1)N^2} > 0$ on both sides of (39), it yields

$$\begin{aligned} & \frac{\lambda_D(\boldsymbol{\theta}_D^{**})\lambda_U(\boldsymbol{\theta}_U^{**})(\tilde{L}_1(\boldsymbol{\theta}_U^{**}, \boldsymbol{\theta}_D^{**}) - L_1(\boldsymbol{\theta}_U^*, \boldsymbol{\theta}_D^*))}{3(2^{\gamma_D} - 1)\sigma_A^2(2^{\gamma_A} - 1)N^2} \\ & \geq \frac{\kappa_U\lambda_D(\boldsymbol{\theta}_D^{**})(2^{\gamma_A} - 1)}{6(2^{\gamma_D} - 1)N^2} + \frac{\kappa_A\lambda_U(\boldsymbol{\theta}_U^{**})(2^{\gamma_D} - 1)\sigma_D^2}{6(2^{\gamma_A} - 1)\sigma_A^2N^2} - \frac{\kappa_A(|g|^2 + |\mathbf{f}_{DU}^H \boldsymbol{\theta}_U^{**}|^2 + |\mathbf{g}_{DU}^H \boldsymbol{\theta}_D^{**}|^2)}{N^2} \\ & \geq \frac{\kappa_U(|h_{DA}|^2 + |\mathbf{g}_{DA}^H \boldsymbol{\theta}_D^{**}|^2 - 2|h_{DA}||\mathbf{g}_{DA}^H \boldsymbol{\theta}_D^{**}|)(2^{\gamma_A} - 1)}{6(2^{\gamma_D} - 1)N^2} \\ & \quad + \frac{\kappa_A(|h_{AU}|^2 + |\mathbf{f}_{AU}^H \boldsymbol{\theta}_U^{**}|^2 - 2|h_{AU}||\mathbf{f}_{AU}^H \boldsymbol{\theta}_U^{**}|)(2^{\gamma_D} - 1)\sigma_D^2}{6(2^{\gamma_A} - 1)\sigma_A^2N^2} \\ & \quad - \frac{\kappa_A(|g|^2 + |\mathbf{f}_{DU}^H \boldsymbol{\theta}_U^{**}|^2 + |\mathbf{g}_{DU}^H \boldsymbol{\theta}_D^{**}|^2)}{N^2} = U(\boldsymbol{\theta}_U^{**}, \boldsymbol{\theta}_D^{**}) - \frac{\kappa_A|g|^2}{N^2}, \end{aligned} \quad (40)$$

where the second inequality holds due to the fact that

$$\lambda_U(\boldsymbol{\theta}_U^{**}) \triangleq |h_{AU} + \mathbf{f}_{AU}^H \boldsymbol{\theta}_U^{**}|^2 \geq (|h_{AU}| - |\mathbf{f}_{AU}^H \boldsymbol{\theta}_U^{**}|)^2 = |h_{AU}|^2 + |\mathbf{f}_{AU}^H \boldsymbol{\theta}_U^{**}|^2 - 2|h_{AU}||\mathbf{f}_{AU}^H \boldsymbol{\theta}_U^{**}|, \quad (41)$$

$$\lambda_D(\boldsymbol{\theta}_D^{**}) \triangleq |h_{DA} + \mathbf{g}_{DA}^H \boldsymbol{\theta}_D^{**}|^2 \geq (|h_{DA}| - |\mathbf{g}_{DA}^H \boldsymbol{\theta}_D^{**}|)^2 = |h_{DA}|^2 + |\mathbf{g}_{DA}^H \boldsymbol{\theta}_D^{**}|^2 - 2|h_{DA}||\mathbf{g}_{DA}^H \boldsymbol{\theta}_D^{**}|. \quad (42)$$

Based on (40), we can guarantee $\tilde{L}_1(\boldsymbol{\theta}_U^{**}, \boldsymbol{\theta}_D^{**}) \geq L_1(\boldsymbol{\theta}_U^*, \boldsymbol{\theta}_D^*)$ if (12) is satisfied.

Moreover, assuming Rayleigh fading channels for all IRS-related links, due to (11), we have $|\mathbf{g}_{DA}^H \boldsymbol{\theta}_D^{**}| = \sum_{n=1}^{(1-\rho)N} |g_{IA,n}| |g_{DI,n}|$ and $|\mathbf{f}_{AU}^H \boldsymbol{\theta}_U^{**}| = \sum_{n=1}^{\rho N} |f_{IU,n}| |f_{AI,n}|$, where $f_{IU,n}$ and $f_{AI,n}$ denote the n -th elements of \mathbf{f}_{IU} and \mathbf{f}_{AI} , respectively, and $g_{IA,n}$ and $g_{DI,n}$ denote the n -th elements of \mathbf{g}_{IA} and \mathbf{g}_{DI} , respectively. Since $|f_{IU,n}|$, $|f_{AI,n}|$, $|g_{IA,n}|$ and $|g_{DI,n}|$ are statistically independent and follow Rayleigh distribution with mean values $\frac{\sqrt{\pi}\varrho_{f_{IU}}}{2}$, $\frac{\sqrt{\pi}\varrho_{f_{AI}}}{2}$, $\frac{\sqrt{\pi}\varrho_{g_{IA}}}{2}$, and $\frac{\sqrt{\pi}\varrho_{g_{DI}}}{2}$, respectively, we have $\mathbb{E}(|f_{IU,n}| |f_{AI,n}|) = \frac{\pi\varrho_{f_{IU}}\varrho_{f_{AI}}}{4}$ and $\mathbb{E}(|g_{IA,n}| |g_{DI,n}|) = \frac{\pi\varrho_{g_{IA}}\varrho_{g_{DI}}}{4}$.

When $N \rightarrow \infty$, we obtain

$$\left| \frac{\mathbf{g}_{DA}^H \boldsymbol{\theta}_D^{**}}{(1-\rho)N} \right| = \frac{\sum_{n=1}^{(1-\rho)N} |g_{IA,n}| |g_{DI,n}|}{(1-\rho)N} \rightarrow \frac{\pi\varrho_{f_{IU}}\varrho_{f_{AI}}}{4}, \quad (43)$$

$$\left| \frac{\mathbf{f}_{AU}^H \boldsymbol{\theta}_U^{**}}{\rho N} \right| = \frac{\sum_{n=1}^{\rho N} |g_{IA,n}| |g_{DI,n}|}{\rho N} \rightarrow \frac{\pi\varrho_{g_{IA}}\varrho_{g_{DI}}}{4}. \quad (44)$$

Similarly, we have

$$\left| \frac{\mathbf{g}_{DA}^H \boldsymbol{\theta}_D^{**}}{N} \right|^2 \rightarrow \frac{\pi^2 \varrho_{fIU}^2 \varrho_{fAI}^2 (1-\rho)^2}{16}, \quad \left| \frac{\mathbf{f}_{AU}^H \boldsymbol{\theta}_U^{**}}{N} \right|^2 \rightarrow \frac{\pi^2 \varrho_{gIA}^2 \varrho_{gDI}^2 \rho^2}{16}. \quad (45)$$

By leveraging the Lindeberg-Lévy central limit theorem [38] and the conclusion in [6], we have $\mathbf{f}_{DU}^H \boldsymbol{\theta}_U^{**} \sim \mathcal{CN}(0, \rho N \varrho_{fIU}^2 \varrho_{fDI}^2)$ and $\mathbf{g}_{DU}^H \boldsymbol{\theta}_D^{**} \sim \mathcal{CN}(0, (1-\rho) N \varrho_{gIA}^2 \varrho_{gIU}^2)$ as $N \rightarrow \infty$, and $\frac{|\mathbf{f}_{DU}^H \boldsymbol{\theta}_U^{**}|^2 + |\mathbf{g}_{DU}^H \boldsymbol{\theta}_D^{**}|^2}{N} \rightarrow \rho \varrho_{fIU}^2 \varrho_{fDI}^2 + (1-\rho) \varrho_{gIA}^2 \varrho_{gIU}^2$. Thus, we obtain that when N becomes asymptotically large, $U(\boldsymbol{\theta}_U^{**}, \boldsymbol{\theta}_D^{**})$ in this condition satisfies (13). This thus completes the proof.

APPENDIX B

PROOF FOR THEOREM 2

By comparing $L_2(\boldsymbol{\theta}_{DU}^*)$ and $\tilde{L}_2(\boldsymbol{\theta}_{DU}^{**})$, we obtain

$$\begin{aligned} & \tilde{L}_2(\boldsymbol{\theta}_{DU}^{**}) - L_2(\boldsymbol{\theta}_{DU}^*) \\ &= \frac{\kappa_U (2^{\gamma_A} + 1)(2^{\gamma_A} - 1) \sigma_A^2}{2|h_{AU}|^2} + \frac{\kappa_A (2^{\gamma_D} + 1)(2^{\gamma_D} - 1) \sigma_D^2}{2\omega_D(\boldsymbol{\theta}_{DU}^{**})} \\ & \quad - \left(\frac{\bar{\gamma}_3}{|h_{AU}|^2} + \frac{\bar{\gamma}_2}{\omega_D(\boldsymbol{\theta}_{DU}^*)} + \frac{\bar{\gamma}_1 \omega_{DU}(\boldsymbol{\theta}_{DU}^*)}{|h_{AU}|^2 \omega_D(\boldsymbol{\theta}_{DU}^*)} \right) \\ & \geq \tilde{L}_2(\boldsymbol{\theta}_{DU}^{**}) - L_2(\boldsymbol{\theta}_{DU}^{**}) \\ &= \frac{\kappa_U (2^{\gamma_A} - 1)^2 \sigma_A^2}{2|h_{AU}|^2} + \frac{\kappa_A (2^{\gamma_D} - 1)^2 \sigma_D^2}{2\omega_D(\boldsymbol{\theta}_{DU}^{**})} - \frac{\bar{\gamma}_1 \omega_{DU}(\boldsymbol{\theta}_{DU}^{**})}{|h_{AU}|^2 \omega_D(\boldsymbol{\theta}_{DU}^{**})}. \end{aligned} \quad (46)$$

Note that $\omega_{DU}(\boldsymbol{\theta}_{DU}^{**}) \triangleq |g + \tilde{\mathbf{g}}_{DU}^H \boldsymbol{\theta}_{DU}^{**}|^2 \leq (|g| + |\tilde{\mathbf{g}}_{DU}^H \boldsymbol{\theta}_{DU}^{**}|)^2 \leq 2(|g|^2 + |\tilde{\mathbf{g}}_{DU}^H \boldsymbol{\theta}_{DU}^{**}|^2)$. Thus, we have

$$\tilde{L}_2(\boldsymbol{\theta}_{DU}^{**}) - L_2(\boldsymbol{\theta}_{DU}^*) \geq \frac{\kappa_U (2^{\gamma_A} - 1)^2 \sigma_A^2}{2|h_{AU}|^2} + \frac{\kappa_A (2^{\gamma_D} - 1)^2 \sigma_D^2}{2\omega_D(\boldsymbol{\theta}_{DU}^{**})} - \frac{2\bar{\gamma}_1 (|g|^2 + |\tilde{\mathbf{g}}_{DU}^H \boldsymbol{\theta}_{DU}^{**}|^2)}{|h_{AU}|^2 \omega_D(\boldsymbol{\theta}_{DU}^{**})}. \quad (47)$$

By multiplying $\frac{|h_{AU}|^2 \omega_D(\boldsymbol{\theta}_{DU}^{**})}{2(2^{\gamma_D} - 1) \sigma_A^2 (2^{\gamma_A} - 1) N^2} > 0$ on both sides of (47) and due to the fact that $\omega_D(\boldsymbol{\theta}_{DU}^{**}) \triangleq |h_{DA} + \tilde{\mathbf{g}}_{DA}^H \boldsymbol{\theta}_{DU}^{**}|^2 \geq (|h_{DA}| - |\tilde{\mathbf{g}}_{DA}^H \boldsymbol{\theta}_{DU}^{**}|)^2 = |h_{DA}|^2 + |\tilde{\mathbf{g}}_{DA}^H \boldsymbol{\theta}_{DU}^{**}|^2 - 2|h_{DA}| |\tilde{\mathbf{g}}_{DA}^H \boldsymbol{\theta}_{DU}^{**}|$, we obtain

$$\begin{aligned} & \frac{|h_{AU}|^2 \omega_D(\boldsymbol{\theta}_{DU}^{**}) (\tilde{L}_2(\boldsymbol{\theta}_{DU}^{**}) - L_2(\boldsymbol{\theta}_{DU}^*))}{2(2^{\gamma_D} - 1) \sigma_A^2 (2^{\gamma_A} - 1) N^2} \\ & \geq \frac{\kappa_U \omega_D(\boldsymbol{\theta}_{DU}^{**}) (2^{\gamma_A} - 1)}{4(2^{\gamma_D} - 1) N^2} + \frac{\kappa_A |h_{AU}|^2 (2^{\gamma_D} - 1) \sigma_D^2}{4(2^{\gamma_A} - 1) \sigma_A^2 N^2} - \frac{\kappa_A (|g|^2 + |\tilde{\mathbf{g}}_{DU}^H \boldsymbol{\theta}_{DU}^{**}|^2)}{N^2} \\ & \geq \frac{\kappa_U (|h_{DA}|^2 + |\tilde{\mathbf{g}}_{DA}^H \boldsymbol{\theta}_{DU}^{**}|^2 - 2|h_{DA}| |\tilde{\mathbf{g}}_{DA}^H \boldsymbol{\theta}_{DU}^{**}|) (2^{\gamma_A} - 1)}{4(2^{\gamma_D} - 1) N^2} + \frac{\kappa_A |h_{AU}|^2 (2^{\gamma_D} - 1) \sigma_D^2}{4(2^{\gamma_A} - 1) \sigma_A^2 N^2} \\ & \quad - \frac{\kappa_A (|g|^2 + |\tilde{\mathbf{g}}_{DU}^H \boldsymbol{\theta}_{DU}^{**}|^2)}{N^2} = U(\boldsymbol{\theta}_{DU}^{**}) - \frac{\kappa_A |g|^2}{N^2}. \end{aligned} \quad (48)$$

Therefore, we can guarantee that the power consumption of the FD system is lower than that of the HD system in Case 2, i.e., $\tilde{L}_2(\boldsymbol{\theta}_{DU}^{**}) \geq L_2(\boldsymbol{\theta}_{DU}^*)$, if the condition (21) is satisfied.

Assuming Rayleigh fading channels for all IRS-related links, when $N \rightarrow \infty$, similarly by leveraging the Lindeberg-Lévy central limit theorem [38], we have $\left| \frac{\tilde{\mathbf{g}}_{DA}^H \boldsymbol{\theta}_{DU}^{**}}{N} \right|^2 \rightarrow \frac{\pi^2 \varrho_{\tilde{g}_{DA}}^2 \varrho_{\tilde{g}_{DU}}^2}{16}$, $\frac{|\tilde{\mathbf{g}}_{DA}^H \boldsymbol{\theta}_{DU}^{**}|}{N^2} \rightarrow 0$, and $\left| \frac{\tilde{\mathbf{g}}_{DU}^H \boldsymbol{\theta}_{DU}^{**}}{N} \right|^2 \rightarrow 0$. Thus, we obtain that when N becomes asymptotically large, $U(\boldsymbol{\theta}_{DU}^{**})$ in this condition satisfies (22). The proof is thus completed.

APPENDIX C

PROOF FOR THEOREM 3

Let us rewrite the expression of the minimum power consumption of the FD system in Case 1 as

$$L_1(\boldsymbol{\theta}_U^*, \boldsymbol{\theta}_D^*) = \frac{\bar{\gamma}_1 \lambda_{DU}(\boldsymbol{\theta}_U^*, \boldsymbol{\theta}_D^*)}{\lambda_D(\boldsymbol{\theta}_D^*) \lambda_U(\boldsymbol{\theta}_U^*)} + \frac{\bar{\gamma}_2}{\lambda_D(\boldsymbol{\theta}_D^*)} + \frac{\bar{\gamma}_3}{\lambda_U(\boldsymbol{\theta}_U^*)}. \quad (49)$$

Based on the Cauchy-Schwarz inequality, we have

$$\lambda_D(\boldsymbol{\theta}_D^{**}) \triangleq |h_{DA} + \mathbf{g}_{DA}^H \boldsymbol{\theta}_D^{**}|^2 \geq (|h_{DA}| - |\mathbf{g}_{DA}^H \boldsymbol{\theta}_D^{**}|)^2 = |h_{DA}|^2 + |\mathbf{g}_{DA}^H \boldsymbol{\theta}_D^{**}|^2 - 2|h_{DA}| |\mathbf{g}_{DA}^H \boldsymbol{\theta}_D^{**}|, \quad (50)$$

$$\lambda_U(\boldsymbol{\theta}_U^{**}) \triangleq |h_{AU} + \mathbf{f}_{AU}^H \boldsymbol{\theta}_U^{**}|^2 \geq (|h_{AU}| - |\mathbf{f}_{AU}^H \boldsymbol{\theta}_U^{**}|)^2 = |h_{AU}|^2 + |\mathbf{f}_{AU}^H \boldsymbol{\theta}_U^{**}|^2 - 2|h_{AU}| |\mathbf{f}_{AU}^H \boldsymbol{\theta}_U^{**}|. \quad (51)$$

Then, with the suboptimal solutions $\boldsymbol{\theta}_U^{**}$ and $\boldsymbol{\theta}_D^{**}$, we further obtain the following inequalities for the minimum power consumption:

$$\begin{aligned} & L_1(\boldsymbol{\theta}_U^*, \boldsymbol{\theta}_D^*) \\ & \leq \frac{\bar{\gamma}_1 \lambda_{DU}(\boldsymbol{\theta}_U^{**}, \boldsymbol{\theta}_D^{**})}{\lambda_D(\boldsymbol{\theta}_D^{**}) \lambda_U(\boldsymbol{\theta}_U^{**})} + \frac{\bar{\gamma}_2}{\lambda_D(\boldsymbol{\theta}_D^{**})} + \frac{\bar{\gamma}_3}{\lambda_U(\boldsymbol{\theta}_U^{**})} \\ & \leq \frac{\bar{\gamma}_1 \lambda_{DU}(\boldsymbol{\theta}_U^{**}, \boldsymbol{\theta}_D^{**})}{(|h_{AU}| - |\mathbf{f}_{AU}^H \boldsymbol{\theta}_U^{**}|)^2 (|h_{DA}| - |\mathbf{g}_{DA}^H \boldsymbol{\theta}_D^{**}|)^2} + \frac{\bar{\gamma}_2}{(|h_{DA}| - |\mathbf{g}_{DA}^H \boldsymbol{\theta}_D^{**}|)^2} + \frac{\bar{\gamma}_3}{(|h_{AU}| - |\mathbf{f}_{AU}^H \boldsymbol{\theta}_U^{**}|)^2} \\ & \leq \tilde{U}(\boldsymbol{\theta}_U^{**}, \boldsymbol{\theta}_D^{**}) \\ & \triangleq \frac{3\bar{\gamma}_1 (|g|^2 + |\mathbf{f}_{DU}^H \boldsymbol{\theta}_U^{**}|^2 + |\mathbf{g}_{DU}^H \boldsymbol{\theta}_D^{**}|^2)}{(|h_{AU}|^2 + |\mathbf{f}_{AU}^H \boldsymbol{\theta}_U^{**}|^2 - 2|h_{AU}| |\mathbf{f}_{AU}^H \boldsymbol{\theta}_U^{**}|) (|h_{DA}|^2 + |\mathbf{g}_{DA}^H \boldsymbol{\theta}_D^{**}|^2 - 2|h_{DA}| |\mathbf{g}_{DA}^H \boldsymbol{\theta}_D^{**}|)} \\ & \quad + \frac{\bar{\gamma}_2}{|h_{DA}|^2 + |\mathbf{g}_{DA}^H \boldsymbol{\theta}_D^{**}|^2 - 2|h_{DA}| |\mathbf{g}_{DA}^H \boldsymbol{\theta}_D^{**}|} + \frac{\bar{\gamma}_3}{|h_{AU}|^2 + |\mathbf{f}_{AU}^H \boldsymbol{\theta}_U^{**}|^2 - 2|h_{AU}| |\mathbf{f}_{AU}^H \boldsymbol{\theta}_U^{**}|}, \end{aligned} \quad (52)$$

where the last inequality holds due to the fact that

$$\begin{aligned} \lambda_{DU}(\boldsymbol{\theta}_U^{**}, \boldsymbol{\theta}_D^{**}) & \triangleq |g + \mathbf{f}_{DU}^H \boldsymbol{\theta}_U^{**} + \mathbf{g}_{DU}^H \boldsymbol{\theta}_D^{**}|^2 \leq (|g| + |\mathbf{f}_{DU}^H \boldsymbol{\theta}_U^{**}| + |\mathbf{g}_{DU}^H \boldsymbol{\theta}_D^{**}|)^2 \\ & \leq 3(|g|^2 + |\mathbf{f}_{DU}^H \boldsymbol{\theta}_U^{**}|^2 + |\mathbf{g}_{DU}^H \boldsymbol{\theta}_D^{**}|^2). \end{aligned} \quad (53)$$

Furthermore, let us rewrite $\tilde{U}(\boldsymbol{\theta}_U^{**}, \boldsymbol{\theta}_D^{**})$ as

$$\begin{aligned} & \tilde{U}(\boldsymbol{\theta}_U^{**}, \boldsymbol{\theta}_D^{**}) \\ & \triangleq \frac{3\bar{\gamma}_1(|g|^2 + N\frac{(\mathbf{f}_{DU}^H \boldsymbol{\theta}_U^{**})^2 + |\mathbf{g}_{DU}^H \boldsymbol{\theta}_D^{**}|^2}{N})}{(|h_{DA}|^2 + N^2\frac{|\mathbf{g}_{DA}^H \boldsymbol{\theta}_D^{**}|^2}{N^2} - 2N|h_{DA}|\frac{|\mathbf{g}_{DA}^H \boldsymbol{\theta}_D^{**}|}{N})(|h_{AU}|^2 + N^2\frac{|\mathbf{f}_{AU}^H \boldsymbol{\theta}_U^{**}|^2}{N^2} - 2N|h_{AU}|\frac{|\mathbf{f}_{AU}^H \boldsymbol{\theta}_U^{**}|}{N})} \\ & + \frac{\bar{\gamma}_2}{|h_{DA}|^2 + N^2\frac{|\mathbf{g}_{DA}^H \boldsymbol{\theta}_D^{**}|^2}{N^2} - 2N|h_{DA}|\frac{|\mathbf{g}_{DA}^H \boldsymbol{\theta}_D^{**}|}{N}} + \frac{\bar{\gamma}_3}{|h_{AU}|^2 + N^2\frac{|\mathbf{f}_{AU}^H \boldsymbol{\theta}_U^{**}|^2}{N^2} - 2N|h_{AU}|\frac{|\mathbf{f}_{AU}^H \boldsymbol{\theta}_U^{**}|}{N}}. \end{aligned} \quad (54)$$

Assuming Rayleigh fading channels for all IRS-related links, similarly when $N \rightarrow \infty$ we obtain

$$\begin{aligned} & \left| \frac{\mathbf{g}_{DA}^H \boldsymbol{\theta}_D^{**}}{N} \right| \rightarrow \frac{\pi \varrho_{gIA} \varrho_{gDI} (1 - \rho)}{4}, \quad \left| \frac{\mathbf{g}_{DA}^H \boldsymbol{\theta}_D^{**}}{N} \right|^2 \rightarrow \frac{\pi^2 \varrho_{gIA}^2 \varrho_{gDI}^2 (1 - \rho)^2}{16}, \quad \left| \frac{\mathbf{f}_{AU}^H \boldsymbol{\theta}_U^{**}}{N} \right| \rightarrow \frac{\pi \varrho_{fIU} \varrho_{fAI} \rho}{4}, \\ & \left| \frac{\mathbf{f}_{AU}^H \boldsymbol{\theta}_U^{**}}{N} \right|^2 \rightarrow \frac{\pi^2 \varrho_{fIU}^2 \varrho_{fAI}^2 \rho^2}{16}, \quad \frac{|\mathbf{f}_{DU}^H \boldsymbol{\theta}_U^{**}|^2 + |\mathbf{g}_{DU}^H \boldsymbol{\theta}_D^{**}|^2}{N} \rightarrow \rho \varrho_{fIU}^2 \varrho_{fDI}^2 + (1 - \rho) \varrho_{gDI}^2 \varrho_{gIU}^2. \end{aligned} \quad (55)$$

Therefore, when N becomes asymptotically large, the upper bound of $L_3(\boldsymbol{\theta}_U^*, \boldsymbol{\theta}_D^*)$ satisfies

$$\begin{aligned} \tilde{U}(\boldsymbol{\theta}_U^{**}, \boldsymbol{\theta}_D^{**}) & \rightarrow \frac{3\bar{\gamma}_1(|g|^2 + N(\rho \varrho_{fIU}^2 \varrho_{fDI}^2 + (1 - \rho) \varrho_{gDI}^2 \varrho_{gIU}^2))}{(|h_{DA}|^2 + \frac{\varpi_g^2}{16} N^2 - \frac{|h_{DA}| \varpi_g}{2} N)(|h_{AU}|^2 + \frac{\varpi_f^2}{16} N^2 - \frac{|h_{AU}| \varpi_f}{2} N)} \\ & + \frac{\bar{\gamma}_2}{|h_{DA}|^2 + \frac{\varpi_g^2}{16} N^2 - \frac{|h_{DA}| \varpi_g}{2} N} + \frac{\bar{\gamma}_3}{|h_{AU}|^2 + \frac{\varpi_f^2}{16} N^2 - \frac{|h_{AU}| \varpi_f}{2} N} \rightarrow 0, \end{aligned} \quad (56)$$

where $\varpi_g \triangleq \pi \varrho_{gIA} \varrho_{gDI} (1 - \rho)$ and $\varpi_f \triangleq \pi \varrho_{fIU} \varrho_{fAI} \rho$. Since the last two terms on the right hand side (RHS) of (56) dominate in the magnitude of $\tilde{U}(\boldsymbol{\theta}_U^{**}, \boldsymbol{\theta}_D^{**})$, we can see that $\tilde{U}(\boldsymbol{\theta}_U^{**}, \boldsymbol{\theta}_D^{**})$ decreases quadratically with the increasing of N . The proof is thus completed.

APPENDIX D

PROOF OF EQUIVALENCE BETWEEN (27) AND (28)

By fixing the other variables, the optimum v for minimizing (28) is given by

$$v = \frac{|h_{DA} + \mathbf{g}_{DA}^H \boldsymbol{\theta}_D| |h_{AU} + \mathbf{f}_{AU}^H \boldsymbol{\theta}_U|}{\bar{\gamma}_1 |g + \mathbf{f}_{DU}^H \boldsymbol{\theta}_U + \mathbf{g}_{DU}^H \boldsymbol{\theta}_D|^2 + \bar{\gamma}_2 |h_{AU} + \mathbf{f}_{AU}^H \boldsymbol{\theta}_U|^2 + \bar{\gamma}_3 |h_{DA} + \mathbf{g}_{DA}^H \boldsymbol{\theta}_D|^2}. \quad (57)$$

By substituting (57) into (28), we have the following equivalent optimization problem:

$$\max_{\boldsymbol{\phi}_U, \boldsymbol{\phi}_D} \frac{|h_{DA} + \mathbf{g}_{DA}^H \boldsymbol{\psi}_D|^2 |h_{AU} + \mathbf{f}_{AU}^H \boldsymbol{\psi}_U|^2}{\bar{\gamma}_1 |g + \mathbf{f}_{DU}^H \boldsymbol{\psi}_U + \mathbf{g}_{DU}^H \boldsymbol{\psi}_D|^2 + \bar{\gamma}_2 |h_{AU} + \mathbf{f}_{AU}^H \boldsymbol{\psi}_U|^2 + \bar{\gamma}_3 |h_{DA} + \mathbf{g}_{DA}^H \boldsymbol{\psi}_D|^2}. \quad (58)$$

It is readily seen that (27) is equivalent to (28). This thus completes the proof.

REFERENCES

- [1] C. Liaskos, S. Nie, A. Tsioliaridou, A. Pitsillides, S. Ioannidis, and I. Akyildiz, "A new wireless communication paradigm through software-controlled metasurfaces," *IEEE Commun. Mag.*, vol. 56, no. 9, pp. 162–169, Sep. 2018.
- [2] M. Di Renzo *et al.*, "Smart radio environments empowered by AI reconfigurable meta-surfaces: An idea whose time has come," *EURASIP J. Wireless Commun. Netw.*, May 2019.
- [3] E. Basar, M. Di Renzo, J. De Rosny, M. Debbah, M. Alouini, and R. Zhang, "Wireless communications through reconfigurable intelligent surfaces," *IEEE Access*, vol. 7, pp. 116 753–116 773, Aug. 2019.
- [4] Q. Wu, S. Zhang, B. Zheng, C. You, and R. Zhang, "Intelligent reflecting surface aided wireless communications: A tutorial," *arXiv preprint arXiv:2007.02759*, 2020.
- [5] Q. Wu and R. Zhang, "Towards smart and reconfigurable environment: Intelligent reflecting surface aided wireless network," *IEEE Commun. Mag.*, vol. 58, no. 1, pp. 106–112, Jan. 2020.
- [6] Q. Wu and R. Zhang, "Intelligent reflecting surface enhanced wireless network via joint active and passive beamforming," *IEEE Trans. Wireless Commun.*, vol. 18, no. 11, pp. 5394–5409, Nov. 2019.
- [7] C. Huang, A. Zappone, G. C. Alexandropoulos, M. Debbah, and C. Yuen, "Reconfigurable intelligent surfaces for energy efficiency in wireless communication," *IEEE Trans. Wireless Commun.*, vol. 18, no. 8, pp. 4157–4170, Aug. 2019.
- [8] M. M. Zhao, Q. Wu, M. J. Zhao, and R. Zhang, "Intelligent reflecting surface enhanced wireless network: Two-timescale beamforming optimization," *IEEE Trans. Wireless Commun.*, DOI: 10.1109/TWC.2020.3022297, 2020.
- [9] T. Jiang and Y. Shi, "Over-the-air computation via intelligent reflecting surfaces," in *Proc. IEEE Global Communications Conference (GLOBECOM)*, Dec. 2019, pp. 1–6.
- [10] Y. Yang, B. Zheng, S. Zhang, and R. Zhang, "Intelligent reflecting surface meets OFDM: Protocol design and rate maximization," *IEEE Trans. Commun.*, vol. 68, no. 7, pp. 4522–4535, Jul. 2020.
- [11] J. Zuo, Y. Liu, Z. Qin, and N. Al-Dhahir, "Resource allocation in intelligent reflecting surface assisted NOMA systems," *arXiv preprint arXiv:2002.01765*, 2020.
- [12] A. Sabharwal, P. Schniter, D. Guo, D. W. Bliss, S. Rangarajan, and R. Wichman, "In-band full-duplex wireless: Challenges and opportunities," *IEEE J. Sel. Areas Commun.*, vol. 32, no. 9, pp. 1637–1652, Sep. 2014.
- [13] G. Zheng, "Joint beamforming optimization and power control for full-duplex MIMO two-way relay channel," *IEEE Trans. Signal Process.*, vol. 63, no. 3, pp. 555–566, Feb. 2015.
- [14] T. Riihonen, S. Werner, and R. Wichman, "Mitigation of loopback self-interference in full-duplex MIMO relays," *IEEE Trans. Signal Process.*, vol. 59, no. 12, pp. 5983–5993, Dec. 2011.
- [15] E. Everett, A. Sahai, and A. Sabharwal, "Passive self-interference suppression for full-duplex infrastructure nodes," *IEEE Trans. Wireless Commun.*, vol. 13, no. 2, pp. 680–694, Feb. 2014.
- [16] Z. Zhang, X. Chai, K. Long, A. V. Vasilakos, and L. Hanzo, "Full duplex techniques for 5G networks: Self-interference cancellation, protocol design, and relay selection," *IEEE Commun. Mag.*, vol. 53, no. 5, pp. 128–137, May 2015.
- [17] D. Bharadia, E. McMillin, and S. Katti, "Full duplex radios," in *Proceedings of the ACM SIGCOMM*, 2013, p. 375–386.
- [18] Y. Xin, M. Ma, Z. Zhao, and B. Jiao, "Co-channel interference suppression techniques for full duplex cellular system," *China Communications*, vol. 12, pp. 18–27, Dec. 2015.
- [19] E. Park, J. Bae, H. Ju, and Y. Han, "Resource allocation for full-duplex systems with imperfect co-channel interference estimation," *IEEE Trans. Wireless Commun.*, vol. 18, no. 4, pp. 2388–2400, Apr. 2019.
- [20] J. Zuo, Y. Liu, E. Basar, and O. A. Dobre, "Intelligent reflecting surface enhanced millimeter-wave NOMA systems," *IEEE Commun. Lett.*, DOI: 10.1109/LCOMM.2020.3009158, 2020.
- [21] P. Wang, J. Fang, X. Yuan, Z. Chen, and H. Li, "Intelligent reflecting surface-assisted millimeter wave communications: Joint active and passive precoding design," *IEEE Trans. Veh. Technol.*, DOI: 10.1109/TVT.2020.3031657, 2020.

- [22] M. Cui, G. Zhang, and R. Zhang, "Secure wireless communication via intelligent reflecting surface," *IEEE Wireless Commun. Lett.*, vol. 8, no. 5, pp. 1410–1414, Oct. 2019.
- [23] S. Hong, C. Pan, H. Ren, K. Wang, and A. Nallanathan, "Artificial-noise-aided secure MIMO wireless communications via intelligent reflecting surface," *IEEE Trans. Commun.*, DOI: 10.1109/TCOMM.2020.3024621, 2020.
- [24] Q. Wu and R. Zhang, "Joint active and passive beamforming optimization for intelligent reflecting surface assisted SWIPT under QoS constraints," *IEEE J. Sel. Areas Commun.*, vol. 38, no. 8, pp. 1735–1748, Aug. 2020.
- [25] C. Pan, H. Ren, K. Wang, M. ElKashlan, A. Nallanathan, J. Wang, and L. Hanzo, "Intelligent reflecting surface aided MIMO broadcasting for simultaneous wireless information and power transfer," *IEEE J. Sel. Areas Commun.*, vol. 38, no. 8, pp. 1719–1734, Aug. 2020.
- [26] Y. Zhang, C. Zhong, Z. Zhang, and W. Lu, "Sum rate optimization for two way communications with intelligent reflecting surface," *IEEE Commun. Lett.*, vol. 24, no. 5, pp. 1090–1094, May 2020.
- [27] H. Shen, T. Ding, W. Xu, and C. Zhao, "Beamforming design with fast convergence for IRS-aided full-duplex communication," *arXiv preprint arXiv:2008.00448*, 2020.
- [28] D. Xu, X. Yu, Y. Sun, D. W. K. Ng, and R. Schober, "Resource allocation for IRS-assisted full-duplex cognitive radio systems," *arXiv preprint arXiv:2003.07467*, 2020.
- [29] Y. Han, S. Zhang, L. Duan, and R. Zhang, "Cooperative double-IRS aided communication: Beamforming design and power scaling," *IEEE Wireless Commun. Lett.*, vol. 9, no. 8, pp. 1206–1210, Aug. 2020.
- [30] S. Zhang and R. Zhang, "Intelligent reflecting surface aided multi-user communication: Capacity region and deployment strategy," *arXiv preprint arXiv:2009.02324*, 2020.
- [31] B. Zheng and R. Zhang, "Intelligent reflecting surface-enhanced OFDM: Channel estimation and reflection optimization," *IEEE Wireless Commun. Lett.*, vol. 9, no. 4, pp. 518–522, Apr. 2020.
- [32] Z. He and X. Yuan, "Cascaded channel estimation for large intelligent metasurface assisted massive MIMO," *IEEE Wireless Commun. Lett.*, vol. 9, no. 2, pp. 210–214, Feb. 2020.
- [33] A. Abu Al Haija and C. Tellambura, "Decoding delay and outage performance analysis of full-duplex decode-forward relaying: Backward or sliding window decoding," *IEEE Trans. Commun.*, vol. 64, no. 11, pp. 4520–4533, Nov. 2016.
- [34] Y. Cai, K. Xu, A. Liu, M. Zhao, B. Champagne, and L. Hanzo, "Two-timescale hybrid analog-digital beamforming for mmwave full-duplex MIMO multiple-relay aided systems," *IEEE J. Sel. Areas Commun.*, vol. 38, no. 9, pp. 2086–2103, Sep. 2020.
- [35] D. Bertsekas, *Nonlinear Programming*. 2nd ed. Belmont, MA: Athena Scientific, 1999.
- [36] K. Shen and W. Yu, "Fractional programming for communication systems—part I: Power control and beamforming," *IEEE Trans. Signal Process.*, vol. 66, no. 10, pp. 2616–2630, May 2018.
- [37] M. M. Zhao, Q. Wu, M. J. Zhao, and R. Zhang, "Exploiting amplitude control in intelligent reflecting surface aided wireless communication with imperfect CSI," *arXiv preprint arXiv:2005.07002*, 2020.
- [38] H. Cramér, *Random Variables and Probability Distributions*. Cambridge, U.K.: Cambridge Univ. Press, 2004.